Exchange effects in nucleus–nucleus potentials and nuclear rainbow scattering

Dao Tien Khoa and O. M. Knyaz'kov

Joint Institute for Nuclear Research, Dubna

Fiz. Elem. Chastits At. Yadra **21**, 1456–1498 (November–December 1990)

The semimicroscopic approach to the description of low-energy nucleus–nucleus interactions is described. The real optical potentials and form factors of inelastic transitions are obtained in closed form on the basis of the effective nucleon–nucleon forces and taking into account exchange effects in the density-matrix formalism. The nuclear rainbow phenomenon is discussed. The semimicroscopic approach is used to analyze the data on nuclear rainbow scattering observed in the elastic scattering of α particles and other composite particles, and to study the role of one-nucleon exchange effects in these processes.

INTRODUCTION

The analysis of the scattering of composite particles on nuclei at low energies is an important source of information on the properties of the internuclear potential.[1] Such analyses have been carried out both within the framework of the standard optical model with the potential specified in parametrized form, and with its parameters found by comparing the theoretical and experimental cross sections, and within the framework of the microscopic model, in which the potentials are constructed on the basis of the effective nucleon–nucleon forces.[2] These constructions are not limited to use of only the double convolution procedure, but include multiparticle nucleon–nucleon correlations modeled by the density dependence of the effective forces,[3] and also exchange nucleon–nucleon correlations due to the Pauli principle.[3,4]

The explicit inclusion of nucleon–nucleon correlations in the formalism of the theory makes it possible to refine the form of the nucleus–nucleus potential, and also to improve its behavior in the surface and interior regions of the target nucleus. For a long time it was assumed that the cross sections for elastic scattering of α particles and heavy ions on nuclei are sensitive to the behavior of the potential at the strong-absorption radius (R_{SA}).[2] However, the discovery of the nuclear rainbow (NR) effect[5,6] in the scattering of α particles on nuclei showed that the angular distributions of elastically scattered α particles at angles larger than the nuclear rainbow scattering angle are sensitive to the behavior of the potential at distances smaller than R_{SA}. This made it possible to uniquely determine the α-particle potentials for each of the target nuclei studied in Ref. 6. In relation to this, it is of particular interest to construct the nucleus–nucleus potential in the microscopic approach on the basis of the effective nucleon–nucleon forces and with explicit inclusion of correlations.

At low energies exchange correlations are the most important. The systematic inclusion of antisymmetrization effects in nucleus–nucleus potentials is possible using the resonating-group method,[7] but this method is limited to only light projectile and target nuclei for which $A \leqslant 40$ and, in addition, $A = 4n$. A universal method of studying one-nucleon exchange effects is the density-matrix method,[8] which has been widely used in nucleon–nucleus scattering problems and only in isolated cases for constructing α-particle[9,10] and heavy-ion[11] potentials. The recently developed iterationless scheme of calculating exchange terms in nucleus–nucleus potentials[12,13] makes it possible to analyze the properties of these potentials and the scattering cross sections in a wide range of energies. It thus becomes possible to study the energy dependence of the potential "geometry" and, therefore, to study the factors determining the behavior of the potential in the surface region and leading to the appearance of NR effects in elastic scattering.

In addition to the experimental data on elastic scattering, there are measurements of the angular distributions in inelastic and quasielastic processes. In addition to improving the properties of nucleus–nucleus potentials, such data can also be used to verify the transition nuclear densities constructed using semimicroscopic nuclear models.

The aim of the present study is to analyze the theoretical schemes for taking into account one-nucleon exchange effects in the construction of nucleus–nucleus potentials and to use this analysis as the basis for studying the manifestation of NR effects in elastic and inelastic scattering. In Sec. 1 we discuss the choice of the effective nucleon–nucleon forces and the principal methods of constructing exchange terms in nucleus–nucleus potentials. The theoretical formalism of the density-matrix method is described in Sec. 2. There we give the results of potential calculations, study the energy dependence of the potential "geometry," and make a comparison with the zero-range pseudopotential approximation[14] and the data of an empirical analysis. In Sec. 3 we discuss some features of the manifestation of the NR phenomenon and the results of a macroscopic analysis. The results of analyzing the experimental data on elastic and inelastic scattering in the density-matrix formalism are given in Sec. 4. In the Conclusion we summarize our main results and conclusions.

1. EFFECTIVE NUCLEON–NUCLEON FORCES AND INCLUSION OF EXCHANGE EFFECTS IN NUCLEUS–NUCLEUS POTENTIALS

In recent years the M3Y effective NN interaction[15] has been widely used for the microscopic analysis of the scattering of composite particles with energies of up to tens of MeV/nucleon on nuclei. This interaction is based on the G-matrix elements of the Reid and Elliott interactions. The direct (v_D) and exchange (v_E) components of the effective NN interaction are found from the expression[1]

$$V_{D\,(E)} = 1/16\ (3v^c_{TE} + 3v^c_{SE} \pm 9v^c_{T0} \pm v^c_{S0}),$$

where the even (v^c_{TE},v^c_{SE}) and odd (v^c_{T0},v^c_{S0}) triplet and singlet components of the central forces are taken from Ref. 15. As a result, we have

 0090-4759/90/060623-20$04.00

$$v_D(s) = 7999{,}0\,\frac{\exp(-4s)}{4s} - 2134{,}25\,\frac{\exp(-2{,}5s)}{2{,}5s}; \quad (1)$$

$$v_E(s) = 4631{,}4\,\frac{\exp(-4s)}{4s} - 1787{,}1\,\frac{\exp(-2{,}5s)}{2{,}5s} - 7{,}8474\,\frac{\exp(-0{,}7072s)}{0{,}7072s}. \quad (2)$$

The exchange part contains the contribution from the one-pion exchange potential [last term in (2)]; in the direct part this contribution is zero.

Later, a different version of the M3Y effective interaction was introduced. It is constructed on the *G*-matrix element of the so-called "Paris" potential.[16] In this case we obtain the following for the direct and exchange components, respectively:

$$v_D(s) = 11061{,}6\,\frac{\exp(-4s)}{4s} - 2537{,}5\,\frac{\exp(-2{,}5s)}{2{,}5s}; \quad (3)$$

$$v_E(s) = -1524{,}0\,\frac{\exp(-4s)}{4s} - 518{,}8\,\frac{\exp(-2{,}5s)}{2{,}5s} - 7{,}8474\,\frac{\exp(-0{,}7072s)}{0{,}7072s}. \quad (4)$$

Comparing Eqs. (1), (2) and (3), (4), we see that for the Paris potential the exchange component is more attractive than for the Reid–Elliott interaction, while the contribution from the one-pion exchange potential is the same in both cases. Below, we shall show that the direct part of the potential constructed on the Paris potential is completely repulsive, with attraction arising only from the exchange component.

Let us consider the interaction of an incident composite particle with a target nucleus. In first order in the effective *NN* forces the interaction potential can be written as

$$U(\mathbf{R}) = U^D(\mathbf{R}) + U^E(\mathbf{R}). \quad (5)$$

Here the first term is the direct potential of the double-convolution model:

$$U^D(\mathbf{R}) = \int\int \rho^{(1)}(\mathbf{r}_1)\, v_D(\mathbf{s})\, \rho^{(2)}(\mathbf{r}_2)\, d\mathbf{r}_1 d\mathbf{r}_2,\ \mathbf{s} = \mathbf{r}_2 - \mathbf{r}_1 - \mathbf{R}, \quad (6)$$

where $\rho^{(i)}(\mathbf{r}_i)$ are the densities of the colliding nuclei. The enormous computational difficulties associated with the calculation of the second (exchange) term in (5) led over time to the neglect of this second term, i.e., it was assumed that $v_E(s) = 0$, and instead a zero-range pseudopotential was introduced into $v_D(s)$ (Ref. 14). In this case instead of (1) we obtain

$$v'_D(s) = 7999{,}0\,\frac{\exp(-4s)}{4s} - 2134{,}25\,\frac{\exp(-2{,}5s)}{2{,}5s} + \hat{J}_{00}(E)\,\delta(s); \quad (7)$$

$$\hat{J}_{00}(E) = -276\,(1 - 0{,}005\,E/A).$$

The effective interaction (7) has been widely and successfully used to analyze the elastic scattering of heavy ions on nuclei.[2] We note that this interaction is independent of the matter density distribution in the nucleus. It is averaged over some range of density variation and can be viewed as corresponding to the average value of the density, 1/3 of the value of the normal nuclear-matter density ρ_0. The energy dependence of the M3Y interaction (7) is unimportant for heavy ions, but this is not completely valid for light projectiles at high energies.

The increased amount of experimental data—wider angular and energy ranges, the inclusion of light projectiles, in particular, α particles, in the analysis, and also data on inelastic scattering—has made it necessary to use an M3Y interaction which explicitly depends on the matter density distribution in the nucleus.[17] This is referred to as the DDM3Y interaction, and is constructed in a form factorized in the coordinate and density dependences:

$$v(s, \rho) = v'_D(s)\, f(\rho), \quad (8)$$

where $v'_D(s)$ is the direct part of the M3Y interaction with the addition of a zero-range pseudopotential, and the factor with the density dependence is given by

$$f(\rho) = C_\rho(E)\,(1 + \alpha(E)\exp[-\beta(E)(\rho_1 + \rho_2)]). \quad (9)$$

The parameters C_ρ, α, and β are found by comparing the space integrals of (8), after their substitution into (9), with the space integrals of the *G*-matrix elements constructed in nuclear-matter theory.[18] The values of these parameters for α-particle energies in the range from 28 to 140 MeV are given in Table I. It can be seen that all the quantities display monotonic behavior as a function of energy, except for α at low energies. Analysis of the data of Table I shows that all the parameters have a stronger energy dependence than the pseudopotential constant $\hat{J}_{00}$. For example, the parameter *C*, which is essentially the renormalization parameter of the M3Y interaction [see Eq. (8)], varies by 37% in

TABLE I. Parameters of the DDM3Y effective interaction.

E/A, MeV/nucleon	7	10	15	20	25	29,5	35
C	0,444	0,420	0,405	0,380	0,354	0,336	0,279
α	4,10	4,24	4,21	4,25	4,37	4,39	5,14
β, F^3	10,67	10,15	9,66	9,12	8,54	8,05	7,20
$-\hat{J}_{00}$, MeV·F^3	265,6	262,2	255,3	248,4	241,5	234,6	227,7

the given energy range, whereas $\hat{J}_{00}$ varies by only 14%. This strong energy dependence also means that the additional normalization factor (see below) in DDM3Y potentials no longer depends on the energy.

The elastic scattering of α particles of energy 140 MeV on the nuclei ^{40}Ca, ^{46,48,50}Ti, ^{58}Ni, ^{90}Zr and of energy 172 MeV on the isotopes ^{58,60,62,64}Ni was described successfully in Ref. 17 using the DDM3Y interaction with the introduction of a normalization factor $\lambda \simeq 1.3$. This description was extended to the case of elastic scattering of α particles at energies $E_\alpha = 25$–120 MeV, and also to inelastic scattering with excitation of low-lying states of the target nucleus. In contrast to the M3Y interaction, the introduction of the density dependence into the DDM3Y interaction allows exchange effects due to the Pauli principle to be included at the semiphenomenological level. However, further analysis[19] has shown that it is impossible to use the DDM3Y interaction to describe the scattering of both α particles and heavy ions on nuclei with a single normalization factor.

In order to explicitly include exchange effects in the construction of the nucleus–nucleus potential, we shall start, in the terminology of Ref. 10, from first principles and treat $U^E(\mathbf{R})$ in the density-matrix formalism. The exchange term is the antisymmetrized matrix element

$$U^E = \sum_{\substack{i\in 1\\ j\in 2}} \langle ij|v_E|ji\rangle,$$

where $|i\rangle$ and $|j\rangle$ are the one-particle wave functions of the nucleons in the colliding nuclei. The localized form of the exchange term is[20]

$$U^E(\mathbf{R}) = \int\int \rho^{(1)}(\mathbf{r}_1, \mathbf{r}_1 + \mathbf{s})\, v^E(\mathbf{s})\, \rho^{(2)}(\mathbf{r}_2, \mathbf{r}_2 - \mathbf{s}) \times \exp[i\,\mathbf{k}(\mathbf{R})\,\mathbf{s}/\zeta)]\, d\mathbf{r}_1\, d\mathbf{r}_2, \quad (10)$$

where the local momentum $k(\mathbf{R})$ is given by

$$k^2(\mathbf{R}) = (2m\zeta/\hbar^2)[E - U(\mathbf{R}) - V^C(\mathbf{R})],\ \zeta = A_1A_2/(A_1 + A_2). \quad (11)$$

In (10), $\rho^{(i)}(\mathbf{r},\mathbf{r}')$ are the density matrices of the colliding nuclei:

$$\rho^{(i)}(\mathbf{r}, \mathbf{r}') = \sum_k \varphi_k^*(\mathbf{r})\, \varphi_k(\mathbf{r}'), \quad (12)$$

and $V^C(\mathbf{R})$ is the Coulomb potential. In obtaining the localized form (10) we used the plane-wave approximation.[20,21] As was noted in Ref. 21, where an extremely simplified version was used for the density matrix, this approximation is fully justified in the description of peripheral collisions, in which the densities of the colliding nuclei overlap weakly. Terms of second order in the effective interaction in (5) were neglected for the same reason. The renormalization of the effective NN forces introduced in the comparison of the theoretical calculations with the experimental data to some degree compensates for the neglect of these factors.

To calculate the exchange term it is necessary to specify the explicit form of the density matrices $\rho^{(i)}(\mathbf{r},\mathbf{r}')$. The direct construction of $\rho^{(i)}(\mathbf{r},\mathbf{r}')$ on the basis of the single-particle wave functions [see (12)] is a rather awkward procedure (see, for example, Ref. 22), and therefore in the literature one commonly finds the so-called Slater expression for $\rho(\mathbf{r},\mathbf{r}')$ (Ref. 23):

$$\rho(\mathbf{r},\ \mathbf{r}+\mathbf{s}) = \rho(\mathbf{r}+\mathbf{s}/2)\,\hat{j}_1(k_{\text{eff}}(\mathbf{r}+\mathbf{s}/2)\,s), \quad (13)$$

where

$$\hat{j}_1(x) = 3(\sin x - x\cos x)/x^3; \quad (14)$$

$$k^2_{\text{eff}}(\mathbf{r}) = \frac{5}{3\rho(\mathbf{r})}\left[0{,}6k_F^2(\mathbf{r})\,\rho(\mathbf{r}) + \frac{(\nabla\rho(\mathbf{r}))^2}{36\rho(\mathbf{r})} + \frac{\nabla^2\rho(\mathbf{r})}{12}\right]. \quad (15)$$

Expression (15) for k_{eff} corresponds to the use of the extended Thomas–Fermi approximation for the kinetic-energy density associated with the nucleon motion in the nucleus. Here

$$k_F^2(\mathbf{r}) = [(3/2)\,\pi^2\rho(\mathbf{r})]^{2/3}. \quad (16)$$

For infinite nuclear matter the surface terms in (16) are zero and $k_{\text{eff}}(\mathbf{r}) = k_F(\mathbf{r})$, which corresponds to the Slater approximation.[24] We note that the choice of k_{eff} in the form (15) leads to calculations using (13), (14) of $\rho(\mathbf{r},\mathbf{r}+\mathbf{s})$ which are close to the density matrix obtained when realistic single-particle wave functions are used.[23]

Substituting (13) into (10) and making the corresponding coordinate replacement,[9,10] we find

$$U^E(\mathbf{R}) = \int\int \rho^{(1)}(\mathbf{r})\,\hat{j}_1(k_{\text{eff}\,1}(\mathbf{r})\,s)\,v_E(s)\,\rho^{(2)}(\mathbf{r}-\mathbf{R}) \times \hat{j}_1(k_{\text{eff}\,2}(\mathbf{r}-\mathbf{R})\,s)\exp[i\,\mathbf{k}(\mathbf{R})\,s/\zeta]\,d\mathbf{r}ds. \quad (17)$$

Equations (5), (6), and (17) provide the basis for the construction of nucleus–nucleus potentials taking into account exchange effects. We note that in the density-matrix formalism presented here, only one-nucleon exchange effects are included. The treatment of n-nucleon exchange ($n \geqslant 2$) in this formalism is an extremely complicated problem and so far has not been considered. However, the question of the contribution of n-nucleon exchange has been studied intensively using the resonating-group method. We shall mention only recent studies and their results. It has been shown[25,26] that the main contribution to the exchange terms of nucleus–nucleus potentials comes from one-nucleon exchange effects, and also core exchange effects (exchange of four nucleons in the case of α-particle interactions with nuclei). However, the contribution of core exchange effects decreases with increasing mass difference of the colliding nuclei.[25] Therefore, in the case of the interaction of α particles or other light ions with intermediate and heavy nuclei, in the construction of exchange potentials we can restrict ourselves to the inclusion of one-nucleon exchange effects.

2. EXCHANGE POTENTIALS IN THE DENSITY-MATRIX FORMALISM

In Refs. 9 and 10 the density-matrix formalism was used to construct α-particle potentials, and in Ref. 11 it was generalized to the case of interactions between heavy ions and nuclei. Let us consider the computational scheme of Ref. 9. Preserving the required accuracy in the calculation of

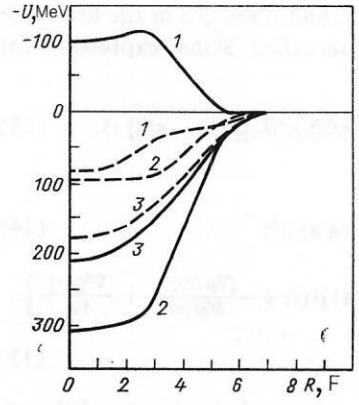

FIG. 1. M3Y potentials in the system $\alpha + {}^{58}$Ni at $E_\alpha = 172.5$ MeV, constructed on the basis of the Paris (solid lines) and Reid–Elliott (dashed lines) interactions: 1) direct potential; 2) exchange potential; 3) total potential.

$U^E(\mathbf{R})$ using (17), in (17) we can expand the terms containing Bessel functions and Yukawa form factors while calculating their Fourier transforms. As a result we will have[9]

$$U^E(\mathbf{R}) = \int \rho^{(1)}(\mathbf{r})\,\rho^{(2)}(\mathbf{r}-\mathbf{R}) \sum_{i=1}^{3} I_i(\mathbf{r},\ \mathbf{r}-\mathbf{R})\,d\mathbf{r}; \qquad (18)$$

$$I_i(\mathbf{r},\ \mathbf{r}-\mathbf{R}) = \frac{4\pi v_i}{(k/\zeta)\,\alpha_i} \sum_{\substack{n,\ m \\ -1,\ -1}} (-)^{n+m} \frac{36nm\,(2n+2m-4)!}{(2n+1)!\,(2m+1)!} k_{F1}^{2n-2} k_{F2}^{2m-2}$$

$$\times [\alpha_i^2 + (k/\zeta)^2]^{3/2-(n+m)} \sin\left\{(2n+2m-3)\left(\tan\frac{k}{\zeta\alpha_i}\right)^{-1}\right\},$$

$$i = 1,\ 2; \qquad (19)$$

$$I_3(\mathbf{r},\ \mathbf{r}-\mathbf{R}) = \frac{4\pi v_3}{\alpha_3[\alpha_3^2 + (k/\zeta)^2]}[1{,}0 - 0{,}07\,(k_{F1}^2 + k_{F2}^2)/(k/\zeta)^2]. \qquad (20)$$

Here α_i are the inverses of the radii of the Yukawa form factors, and k_{F1} and k_{F2} depend on the arguments $\mathbf{r}$ and $\mathbf{r}-\mathbf{R}$, respectively. In this expansion method the integral over s is calculated analytically using Fourier transformation, which leads to expressions of the type $[\alpha_i^2 + (k/\zeta)^2]^{-n}$. In Eqs. (19) and (20), v_i are the force constants of the Yukawa form factors [see (2)]. Analysis of expression (19) shows that in $\Sigma_{n,m}$ it is sufficient to restrict ourselves to terms with $n = m = 3$.

It is not difficult to see that for constant k_{F1} and k_{F2} the quantity $I(\mathbf{r},\mathbf{r}-\mathbf{R})$ is also constant. Therefore, in this case (18) reduces to (6), into which the expression for the zero-range pseudopotential is substituted instead of $v_E(\mathbf{s})$. The energy dependence of the pseudopotential is determined by the energy dependence of k. From this it can be concluded that the pseudopotential approximation for including exchange effects [see (7)] corresponds to a representation of the matter distribution in the nucleus as a distribution in infinite nuclear matter with constant density. The inclusion of the dependence of k_{F1} and k_{F2} on the density (15) leads to an effective exchange interaction which also depends on the density. The exchange potential $U^E(\mathbf{R})$ constructed from first principles possesses the properties characteristic of the semiphenomenological DDM3Y interaction: the energy dependence and "internal" density dependence.

The formalism described here and the effective NN interactions (1)–(2), (3)–(4) were used in Ref. 9 to construct the potentials for interactions of 172.5-MeV α particles with the target nucleus ^{58}Ni. The representations from Refs. 27 and 17, respectively, were used for the matter density distributions in the α particle and in ^{58}Ni. The results of the calculation are shown in Fig. 1. As was noted above, the direct part constructed on the Paris potential is repulsive. This is related to the fact that, in contrast to the Reid–Elliott potential, the Paris potential has a nonzero short-range component in the triplet odd state. Therefore, the attractive part of the α-particle potential is due solely to the contribution of the exchange term. It can be seen from Fig. 1 that the full potential constructed with the Paris effective interaction is deeper than the α-particle potential based on the Reid–Elliott effective interaction. However, in the surface region ($R > 5$ F) the potentials for the two effective interactions become similar.

The α-particle potentials constructed with inclusion of exchange effects were used in Ref. 10 to analyze the elastic scattering of α particles on a group of nuclei. The following target nuclei were used: ^{40}Ca ($E_\alpha = 141.7$ MeV), ^{52}Cr (104.0), ^{50}Ti (104.0), ^{58}Ni (172.5), and ^{208}Pb (140.0). The results of the analysis are given in Table II. In all cases the description of the experimental cross sections is satisfactory.

TABLE II. Optical potentials for the scattering of α particles on the nuclei ^{40}Ca, ^{50}Ti, ^{52}Cr, ^{58}Ni, and ^{208}Pb.

Nucleus	E_{lab}, MeV	λ	$-U_0$, MeV	J_R, MeV·F^3	$\langle r^2\rangle^{1/2}$, F	$-W_v$, MeV	r_v, F	a_v, F	χ^2/F
^{50}Ti	104,0	0,80	189,5	295,0	4,32	22,55	1,539	0,599	11,2
^{52}Cr	104,0	0,80	190,0	296,2	4,36	25,64	1,496	0,660	5,5
^{58}Ni	172,5	0,76	179,1	252,5	4,46	23,50	1,467	0,745	20,6
^{208}Pb	140,0	0,84	195,0	292,4	6,19	20,54	1,484	0,755	25
^{40}Ca	141,7	0,80	171,2	283,7	4,18	22,41	1,529	0,706	53,7
^{58}Ni *	172,5	0,64	210,1	242,2	4,43	22,49	1,453	0,792	35,6

*Analysis with M3Y potential constructed on the basis of the Paris interaction.

We note that the computational scheme based on the general equation (17) or a specific realization of it [see (18)–(20)] has limitations. It follows from expressions (5), (10), and (11) that the construction of $U^E(\mathbf{R})$ requires an awkward iteration procedure, since the desired quantity also enters into the right-hand side of (10) via the momentum $k(\mathbf{R})$; a six-dimensional integral must be computed at each step of the iteration. For describing inelastic transitions (in Refs. 9–11 only the potentials were calculated and elastic scattering was analyzed) a similar procedure is also required to find the inelastic-transition form factors (ITFFs). As the number of coupled channels grows, the amount of machine time required increases dramatically. In Ref. 28 it was also pointed out that the iteration procedure for calculating the exchange potential is too complicated for serious studies of the nuclear densities in a model-independent analysis (MIA) to be carried out using such potentials. Moreover, when the phonon model is used for the target nucleus, it is necessary to construct the phonon representation of the interaction of the incident particle with the target nucleus (this difficulty arises already in the nucleon–nucleus scattering problem), which requires the expansion of the interaction in phonon operators.[29] It is therefore desirable to have a computational scheme in which the optical potential (OP) and the ITFFs are obtained in closed form, without using an iteration procedure.

To solve this problem it is convenient, after transforming (17), to go to the momentum representation. First we integrate over the angles of the vector $\mathbf{s}$ in (17). We have[13]

$$U^E(\mathbf{R}) = 4\pi \int\int_0^\infty f^{(1)}(\mathbf{r}, s)\, f^{(2)}(\mathbf{r}-\mathbf{R}, s) \times v_E(s)\, j_0(k(\mathbf{R})\, s/\zeta)\, s^2\, ds\, d\mathbf{r}, \tag{21}$$

where

$$f^{(i)}(\mathbf{r}, s) = \rho^{(i)}(\mathbf{r})\, \hat{j}_1(k_{\text{eff}\,i}(\mathbf{r})\, s). \tag{22}$$

Taking the Fourier transform, we obtain

$$\int f^{(1)}(\mathbf{r}, s)\, f^{(2)}(\mathbf{r}-\mathbf{R}, s)\, d\mathbf{r} = 1/(2\pi)^3 \int \tilde{f}^{(1)}(-\mathbf{t}, s)\, \tilde{f}^{(2)}(\mathbf{t}, s) \exp(i\mathbf{t}\mathbf{R})\, d\mathbf{t}. \tag{23}$$

Here

$$\tilde{f}^{(i)}(\mathbf{t}, s) = \int f^{(i)}(\mathbf{r}, s) \exp(i\mathbf{t}\mathbf{r})\, d\mathbf{r}. \tag{24}$$

We expand the local densities in multipole series:

$$\rho(\mathbf{r}) = \sum_{\lambda\mu} C_\lambda \rho_\lambda(r)\, Y^*_{\lambda\mu}(\hat{\mathbf{r}}), \tag{25}$$

where $C_\lambda = 1$ for $\lambda \neq 0$ and $C_0 = \sqrt{4\pi}$ (Ref. 1).

Expanding all quantities in (23) and (24) also in multipoles and using (25), we have

$$\int f^{(1)}(\mathbf{r}, s)\, f^{(2)}(\mathbf{r}-\mathbf{R}, s)\, d\mathbf{r} = \sum_{\lambda\mu} C_\lambda G_{\lambda\mu}(R, s)\, Y^*_{\lambda\mu}(\hat{\mathbf{R}}); \tag{26}$$

$$G_{\lambda\mu}(R, s) = (C_{\lambda_1} C_{\lambda_2}/\sqrt{4\pi})\, i^{\lambda_1-\lambda_2-\lambda} \left[\frac{(2\lambda_1+1)(2\lambda_2+1)}{2\lambda+1}\right]^{1/2} \times \langle\lambda_1\mu_1\lambda_2\mu_2|\lambda\mu\rangle \langle\lambda_1 0\lambda_2 0|\lambda 0\rangle (1/2\pi^2) \times \int_0^\infty f^{(1)}_{\lambda_1}(t, s)\, f^{(2)}_{\lambda_2}(t, s)\, j_\lambda(tR)\, t^2\, dt; \tag{27}$$

$$f^{(i)}_{\lambda_i}(t, s) = 4\pi \int_0^\infty \rho^{(i)}_{\lambda_i}(r)\, \hat{j}_1(k_{\text{eff}\,i}(r)\, s)\, j_{\lambda_i}(tr)\, r^2\, dr. \tag{28}$$

The interaction (6), (21), (26)–(28) can lead both to excitation of one of the colliding nuclei ($\lambda_1 = 0, \lambda_2 \neq 0$; $\lambda_1 \neq 0, \lambda_2 = 0$) and to the mutual excitation of the nuclei ($\lambda_1 \neq 0, \lambda_2 \neq 0$) (it is assumed that momentum transfer occurs in the excitation). Expanding the left-hand side of (21) like (25) and substituting (26)–(28) into (21), we find the following for the exchange part of the ITFF with momentum transfer L:

$$C_L U^E_{LM}(R) = 4\pi \sum_{\lambda\lambda'\mu\mu'} C_\lambda C_{\lambda'} S(L\lambda\lambda';\ \mu\mu') \times \int_0^\infty J_{\lambda'\mu'}(k(R)\, s/\zeta)\, G_{\lambda\mu}(R, s)\, v_E(s)\, s^2\, ds; \tag{29}$$

$$S(L\lambda\lambda';\ \mu\mu') = \left[\frac{(2\lambda+1)(2\lambda'+1)}{4\pi(2L+1)}\right]^{1/2} \langle\lambda\mu\lambda'\mu'|LM\rangle \langle\lambda 0\lambda' 0|L0\rangle; \tag{30}$$

$$C_\lambda J_{\lambda\mu}(k(R)\, s/\zeta) = \int j_0(k(\mathbf{R})\, s/\zeta)\, Y_{\lambda\mu}(\hat{\mathbf{R}})\, d\hat{\mathbf{R}}. \tag{31}$$

In order to obtain closed expressions for $U^E_{LM}(R)$, as in Ref. 30 for the nucleon–nucleus case we use the multiplication theorem for the Bessel function $j_0(k(\mathbf{R})s/\zeta)$ (Ref. 31):

$$j_0(yz) = \sum_{n=0}^\infty \frac{1}{n!}\, j_n(z) \left(\frac{1-y^2}{2} z\right)^n,\ |1-y|^2 < 1. \tag{32}$$

Taking into account (5) and (11), we define y and z as follows:

$$y = [k_0^2(R) - k_1^2(\mathbf{R})]^{1/2}/|k_0(R)|,\ z = |k_0(R)|\, s/\zeta; \tag{33}$$

$$k_0^2(R) = (2m\zeta/\hbar^2)[E - U_0^D(R) - V_0^C(R)]; \tag{34}$$

$$k_1^2(\mathbf{R}) = (2m\zeta/\hbar^2)\{U_0^E(R) + \sum_{LM}{}' [U^E_{LM}(R) + U^D_{LM}(R) + V^C_{LM}(R)]\, Y^*_{LM}(\hat{\mathbf{R}})\}. \tag{35}$$

Here the prime on the summation sign means that $L \neq 0$, and $k_0(R)$ is the momentum of the relative motion of the colliding nuclei in the case of elastic scattering without any exchange interactions. In some cases of heavy-ion scattering at energies below the Coulomb barrier, we have $k_0^2(R) < 0$,

and the scattering occurs via indirect processes (exchange and tunneling effects). In such cases it is necessary to take into account the Pauli principle exactly in the scattering problem. Using (33)–(35), we can write (32) as

$$j_0(k(\mathbf{R})\,s/\zeta) = \sum_{n=0}^{\infty} \frac{1}{n!}\, j_n(|k_0(R)|s/\zeta) \times \begin{cases} [(k_1^2(\mathbf{R}) - 2k_0^2(R))\,s/(2\zeta|k_0(R)|)]^n, & k_0^2(R) < 0; \\ [k_1^2(\mathbf{R})\,s/(2\zeta k_0(R))]^n, & k_0^2(R) \geqslant 0. \end{cases} \tag{36}$$

It can be seen that for energies of up to several tens of MeV per nucleon the expression in square brackets in (36) is much less than unity for all R. Keeping the first three terms in the expansion (36), we obtain

$$\begin{aligned} U_{LM}(R) &= U_{LM}^D(R) + U_{LM}^E(R) = U_{LM}^D(R) + I_{LM}^{(0)}(R) \\ &+ \varkappa(R)\, I_{LM}^{(1)}(R)\, A_0(R)\,[1 + \varkappa(R)\, I_{00}^{(1)}(R)] \\ &+ \varkappa^2(R)\, I_{LM}^{(2)}(R)\, A_0^2(R) \\ &+ \frac{\varkappa^2(R)}{4\pi} \sum_{\lambda\mu}{}' [I_{\lambda\mu}^{(1)}(R)\, I_{LM}^{(1)}(R) + I_{LM}^{(2)}(R)\, B_{\lambda\mu}(R)]\, B_{\lambda\mu}(R) \\ &+ \varkappa(R) \sum_{\lambda\mu} \sum_{\lambda'\mu'}{}' (C_\lambda/C_L)\, S(L\lambda\lambda';\ \mu\mu') \\ &\times \{I_{\lambda\mu}^{(1)}(R)\, B_{\lambda'\mu'}(R) + \varkappa(R)\, A_0(R) \\ &\times [I_{\lambda\mu}^{(1)}(R)\, I_{\lambda'\mu'}^{(1)}(R) + 2I_{\lambda\mu}^{(2)}(R)\, B_{\lambda'\mu'}(R)] \\ &+ \varkappa(R) \sum_{\lambda_1\mu_1}{}' \sum_{\lambda_2\mu_2}{}' S(\lambda'\lambda_1\lambda_2;\ \mu_1\mu_2)\, I_{\lambda\mu}^{(2)}(R)\, B_{\lambda_1\mu_1}(R)\, B_{\lambda_2\mu_2}(R)\}, \end{aligned} \tag{37}$$

where

$$B_{\lambda\mu}(R) = I_{\lambda\mu}^{(0)}(R) + U_{\lambda\mu}^D(R) + V_{\lambda\mu}^C(R); \tag{38}$$

$$A_0(R) = I_{00}^{(0)}(R) - f_{k_0}(R);\quad \varkappa(R) = m/(|k_0(R)|\hbar^2). \tag{39}$$

Here

$$I_{\lambda\mu}^{(n)}(R) = (4\pi/n!) \int_0^\infty v_E(s)\, j_n(|k_0(R)|s/\zeta)\, G_{\lambda\mu}(R,\ s)\, s^{n+2}\, ds \tag{40}$$

are exchange integrals, and

$$f_{k_0}(R) = \begin{cases} \hbar^2 k_0^2(R)/m\zeta, & k_0^2(R) < 0; \\ 0, & k_0^2(R) \geqslant 0. \end{cases} \tag{41}$$

Equations (37)–(41) for $L = 0$ can be used to calculate the real part of the OP, and for $L \neq 0$ they can be used to calculate the ITFFs. Analysis shows[12,13] that the contribution of terms of third order in $\varkappa(R)$ to the potential is 1–2% on the whole, which is smaller than the uncertainties in the effective NN forces or in the determination of the nuclear densities.[1,2]

Let us discuss this formalism. The calculation of the quantities $U_{LM}^E(R)$ does not require the use of an awkward iteration procedure. Moreover, the quantities $G_{\lambda\mu}(R,s)$ do not depend on the energy. This fact leads to a significant decrease in the computational time needed to analyze the experimental data on scattering in a wide energy range. Comparison of Eqs. (29)–(31) with the analogous expressions for describing nucleon–nucleus scattering[22,30] shows that they have a similar structure. The difference is that for nucleons $\zeta = A/(A+1)$, and the $G_{\lambda\mu}(R,s)$ are not calculated using (27) and (28), but reduce to the corresponding components of the density matrix. Therefore, in this formalism the construction of the OP and the ITFFs for interactions of nucleons with nuclei is a special case of the problem of finding the OP and the ITFFs for composite particles. The formalism described here can in this sense be viewed as a generalization of the semiempirical approach to the description of interactions of low-energy nucleons with nuclei,[30,32] in which the iterationless scheme for calculating the exchange potential was first proposed. The use in (37)–(41) of the transition densities calculated in semimicroscopic models (for example, in the quasiparticle–phonon model[33] (QPM) or in the theory of finite Fermi systems[34]) makes it possible to check these models with regard to their description of states with complex structure. We note that the formalism described here contains a description of the so-called multipole-mixing effect,[22,30] which is absent in the zero-range pseudopotential approximation. In it the L component of the potential is determined not only by the L-component transition density, but also by the λ components with $\lambda \neq L$.

In relation to the fact that the study of the nuclear rainbow effect makes it possible to study potentials at distances smaller than the strong-absorption radius, where the densities of the colliding nuclei can overlap significantly, we should make two comments about our formalism. The first is that in the region where the nuclear densities overlap significantly the neglect of the polarization terms in the potential (terms of second order in the effective interaction) can no longer be canceled by the renormalization of the effective forces or by the introduction of a density dependence into them. Anticipating our later discussion, we note that up to now the nuclear rainbow effect has been reliably established only for light composite particles, so that we can hope that this formalism is adequate for describing the experimental situation.

The second comment is that in the description of inelastic transitions it is necessary to take into account the effect of the interaction of the colliding nuclei on the rearrangement of their spectra of excited states. Again in this case we note that this formalism can be used to describe the inelastic scattering of α particles on nuclei directly, while to describe the inelastic scattering of heavy composite particles on nuclei it is necessary to analyze the problem of the rearrangement of the internal motion of the nucleons.

In order to have the possibility of describing the inelastic scattering of composite particles (for example, α particles) on nuclei with excitation of low-lying vibrational states, it is necessary to construct the interaction of the incident particle with the target nucleus in the phonon representation. For this the density matrix $\rho(\mathbf{r},\mathbf{r}')$ must be expanded in the parameters describing the dynamical deformation of the nucleus. According to (22), in the first approximation the expansion of $\rho(\mathbf{r},\mathbf{r}')$ reduces to an expansion in the dynamical-deformation parameters of the transition densities.

For them we can use one of the standard parametrizations:[1]

$$\rho_{\lambda}(r) = -\beta_{\lambda} r \left(\frac{r}{R_{0\rho}}\right)^{\nu-2} \frac{d\rho(r)}{dr}. \qquad (42)$$

Equations (37)–(41) have been used in Refs. 12, 13, and 35 to analyze the nucleus–nucleus potentials and the contribution of one-nucleon exchange effects to them. In Figs. 2 and 3 we show the results of the calculation, in a wide energy range, of the potentials for the systems $^{12}C + {}^{12}C$ and $^{16}O + {}^{208}Pb$. As the densities $\rho_0(r)$ for ^{12}C and ^{16}O we used the two-parameter Fermi distributions with parameters from Ref. 19, while for ^{208}Pb we calculated $\rho_0(r)$ using the QPM. There were two variants of the potential calculations: one in which the effects of one-nucleon exchange were explicitly included in the density-matrix formalism using the M3Y interaction [see Eqs. (1) and (2)], and the other taking into account exchange effects in the pseudopotential approximation[1)] using the double-convolution model [see Eqs. (6) and (7)]. It can be seen that for both systems the M3Y (PP) potentials are deeper than the M3Y potentials in the interior region, and shallower in the surface region. There are important differences between them in the interior region, and the two potentials are close in the surface region. As the energy increases the differences between the potentials disappear, especially in the surface region. This decrease reflects the fact that as the energy increases the contribution to the potential from exchange nucleon–nucleon correlations due to the action of the Pauli principle decreases.

In Fig. 4 we show the results of calculations of the α-particle potential for the target nuclei ^{58}Ni and ^{90}Zr. In Fig. 4 we also show the potential (solid line) found from the MIA of Ref. 36. We can see that the M3Y (PP) potential is significantly deeper than the M3Y potential in the interior region.

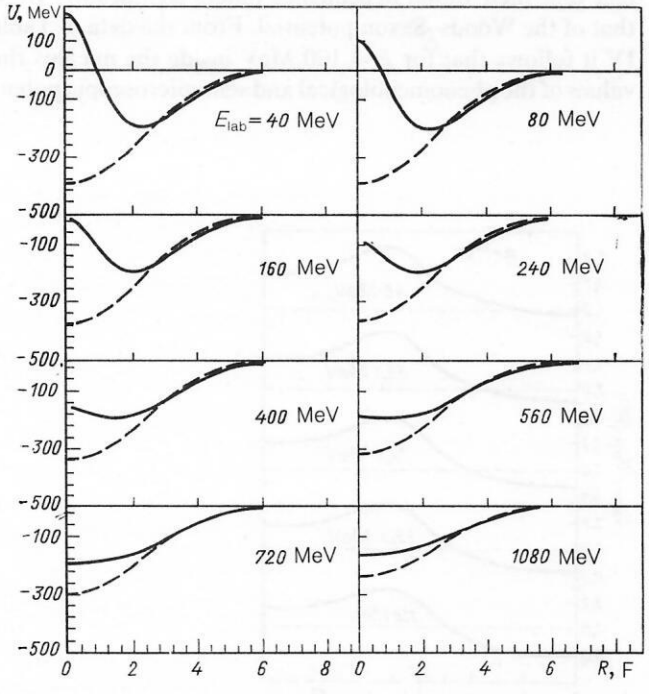

FIG. 2. M3Y potentials (solid lines) and M3Y (PP) potentials (dashed lines) for the system $^{12}C + {}^{12}C$.

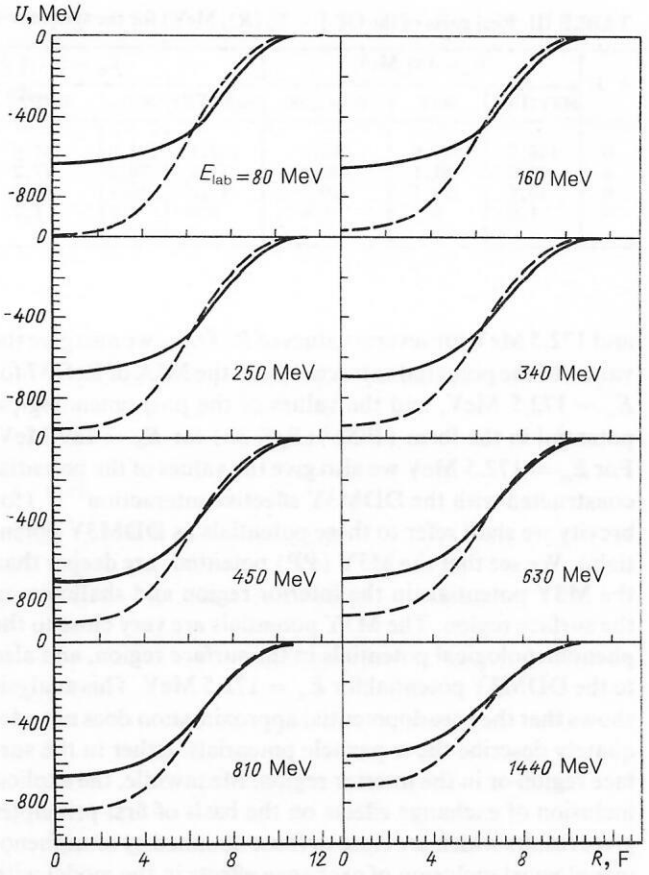

FIG. 3. The same as in Fig. 2 for the system $^{16}O + {}^{208}Pb$.

These potentials are close for $R > 5.5$ F. Meanwhile, the M3Y potential reveals a striking similarity to the spline potential from the MIA in the region $3 < R < 8$ F. In Table III we give the values of the α-particle potentials for $E_{\alpha} = 139$

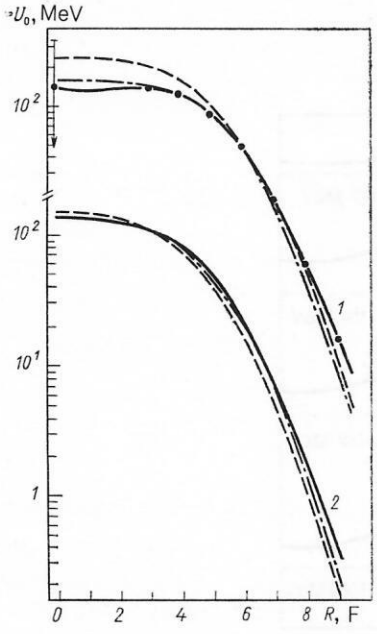

FIG. 4. Potentials for the system $\alpha + {}^{90}Zr$ for $E_{\alpha} = 99.5$ MeV (upper part) and for the system $\alpha + {}^{58}Ni$ for $E_{\alpha} = 139.5$ MeV (lower part): 1) from the MIA of Ref. 36; 2) $(WS)^2$ from Ref. 38; the dashed line is the M3Y (PP) potential, and the dot–dash line is the M3Y potential.

TABLE III. Real parts of the OP [$-U_0(R)$, MeV] for the system $\alpha + {}^{58}$Ni.

R, F	$E_\alpha = 139$ MeV			$E_\alpha = 172{,}5$ MeV			
	M3Y(PP)	M3Y	$(WS)^2$ [38]	M3Y(PP)	M3Y	DDM3Y	MIA [36]
0	146,7	137,9	140,5	137,1	131,0	137,0	50—200
4	76,7	81,1	82,3	71,4	76,2	77,2	81,5
6	16,1	20,1	20,3	15,2	19,1	18,2	20,9
8	1,0	1,2	1,6	0,9	1,2	1,7	1,3

and 172.5 MeV for several values of R. There we also give the values of the potential extracted from the MIA of Ref. 37 for $E_\alpha = 172.5$ MeV, and the values of the phenomenological potential in the form $(WS)^2$ (Ref. 38) for $E_\alpha = 139$ MeV. For $E_\alpha = 172.5$ MeV we also give the values of the potential constructed with the DDM3Y effective interaction[17,18] (for brevity we shall refer to these potentials as DDM3Y potentials). We see that the M3Y (PP) potentials are deeper than the M3Y potentials in the interior region and shallower in the surface region. The M3Y potentials are very close to the phenomenological potentials in the surface region, and also to the DDM3Y potential for $E_\alpha = 172.5$ MeV. This analysis shows that the pseudopotential approximation does not adequately describe the α-particle potentials, either in the surface region or in the interior region. Meanwhile, the explicit inclusion of exchange effects on the basis of first principles gives results which are close to those obtained by semiphenomenological inclusion of exchange effects in the model with the DDM3Y effective interaction.

In Figs. 5–7 we show the ratios of the M3Y and M3Y (PP) potentials as functions of R, constructed for α particles and ^{6}Li and ^{9}Be ions interacting with nuclei at various energies. We see that in all cases the M3Y potentials differ in form from the M3Y (PP) potentials. For α particles the values of these potentials coincide at isolated points for $R < R_{SA}$, while for $E_\alpha \geqslant 100$ MeV the M3Y (PP) potentials, when compared with the M3Y potentials, are deeper in the interior region ($R \sim 2$–4 F) and shallower in the surface region ($R \sim 5$–8 F) (Fig. 5). In the case of α particles interacting with the ^{90}Zr nucleus we can see (Fig. 6) how this regularity develops as the energy increases. For ^{6}Li and ^{9}Be ions the M3Y potentials are more attractive than the M3Y (PP) potentials in both the interior and the surface region of the nucleus. However, after the introduction of the renormalization coefficients for the optimal description of the experimental angular distributions (see Table VIII), the M3Y (PP) potentials, as for α particles, become deeper in the interior region and shallower in the surface region.

Let us study the energy dependence of the potential geometry in more detail. In Table IV we give the results of the calculation of the α-particle potential in the system $\alpha + {}^{90}$Zr for the energy range from 0 to 300 MeV (Ref. 39). In the calculations exchange effects were taken into account in a more approximate form than described above, and the Wildermuth–Schmid effective NN forces[40] with the density dependence of Ref. 32 were used. The potentials constructed in this manner differ from the M3Y potentials (see Sec. 4) in the interior region, but are close to them at the nuclear surface (cf. the value of the potential at $R = 6$ F and $E_\alpha = 100$ MeV in Table IV and in Fig. 4). Therefore, the conclusions about the variation of the potential geometry with energy due to the inclusion of exchange effects are quite general.

A special feature of semimicroscopic potentials is the fact that their radial dependence differs significantly from that of the Woods–Saxon potential. From the data of Table IV it follows that for $E = 100$ MeV inside the nucleus the values of the phenomenological and semimicroscopic poten-

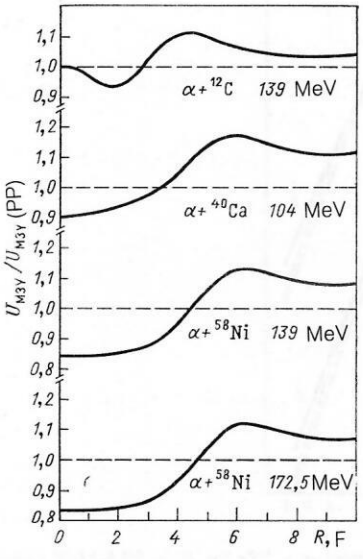

FIG. 5. Radial dependence of the ratios of the unrenormalized M3Y and M3Y (PP) potentials for $\alpha + {}^{12}$C, ^{40}Ca, ^{58}Ni at various energies.

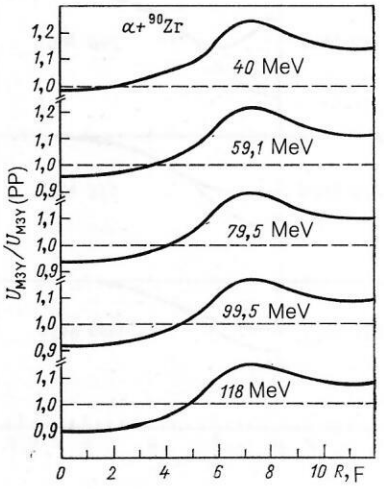

FIG. 6. The same as in Fig. 5 for $\alpha + {}^{90}$Zr for $E_\alpha = 40$–118 MeV.

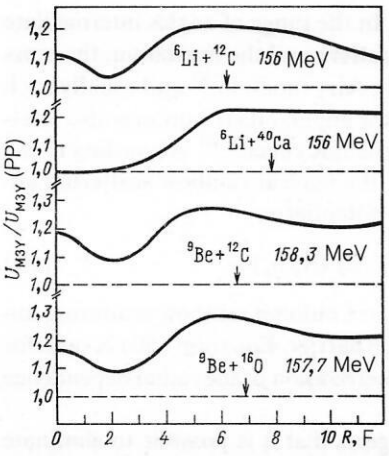

FIG. 7. The same as in Fig. 5 for ^{6}Li + ^{12}C, ^{40}Ca at $E = 156$ MeV and ^{9}Be + ^{12}C, ^{16}O at $E = 158.3$ and 157.7 MeV.

tials differ by almost a factor of 2, whereas this difference is only 5% at the surface.

The constructed potential as a function of energy inside the nucleus can be approximated by the following expressions:

$$-U(E) = U_0 - \gamma E, \quad U_0 = 247\ 8 \text{ MeV}, \quad \gamma = 0{,}15, \tag{43}$$

$$-U(E) = U_0 - \gamma E + \beta E^2,$$

$$\gamma = 0{,}15, \quad \beta = 0{,}00019 \text{ MeV}^{-1}. \tag{44}$$

Equation (43) (the linear approximation) accurately reproduces the potential and its energy-dependent part for $E_\alpha \leqslant 100$ MeV, while in the range $E = 100$–300 MeV the energy-dependent part of the potential is reproduced in the linear approximation with an error reaching 35%. The quadratic approximation [see (44)] is considerably better and reproduces the energy-dependent part of the potential with an accuracy of up to 6%.

Comparison of the data for U_0 and U shows that in the interior of the nucleus the potential depends more weakly on the energy than at the surface. This allows us to write the potential in the form

$$U(R, E) = U_0 [1 - \alpha(R) E] f(R), \tag{45}$$

where $\alpha(R_{1/2}) > \alpha(0)$. From this analysis it follows, for example, that at the radius where the potential falls to half its height $\alpha(R_{1/2}) \simeq 1.7\alpha(0)$, i.e., the contribution of exchange correlations to the energy dependence of the potential is increased by a factor of 1.7, which indicates that exchange correlations are predominantly localized at the nuclear surface. Expression (45) can be interpreted also as the energy dependence of the radius at which the potential falls to half its height $R_{1/2}(E)$. We note that potentials with $R_{1/2}(E)$ have been used for empirical analysis in a number of cases. Several such cases were studied in Ref. 41. For nucleons the dependence $R_{1/2}(E)$ has also been observed in semimicroscopic studies,[32,42,43] while for α particles the question of the energy dependence of $R_{1/2}$ has been studied semiempirically only recently.[39] Following this study, as for the OP depth, we have two possible approximations:

$$R_{1/2}(E) = R_{0\,1/2} - \gamma_R E, \quad \gamma_R = 0{,}001 \text{ F}\cdot\text{MeV}^{-1}, \quad R_{01/2} = 4{,}69 \text{ F}; \tag{46}$$

$$R_{1/2}(E) = R_{0\,1/2} - \gamma_R E + \beta_R E^2,$$

$$\gamma_R = 0{,}0011 \text{ F}\cdot\text{MeV}^{-1}; \quad \beta_R = 0{,}0000012 \text{ MeV}^{-2}\cdot\text{F}. \tag{47}$$

Equation (46), like (43), accurately reproduces $R_{1/2}(E)$ at energies up to $E_\alpha = 100$ MeV, while in the range $E = 100$–300 MeV the error in the energy-dependent part of $R_{1/2}(E)$ reaches 35%. The quadratic approximation (47) works in the entire energy range with an error of up to 1%.

This semimicroscopic analysis therefore confirms the conclusion drawn in the empirical analysis that the radius at which the α-particle OP falls to half its height decreases with increasing energy.[36,44–46] Let us show that dependences of the type (46) introduced into the standard optical model are equivalent to choosing the functional dependence of the potential in the form (45). Expanding the potential $U(R, R_{1/2}(E))$ as a function of $R_{1/2}$ in a Taylor series near the point $R_{1/2} = R_{0,1/2}$, we have

$$U(R, R_{1/2}(E)) = U(R, R_{0\,1/2}) - \gamma(R) E, \tag{48}$$

where

$$\gamma(R) = \gamma_R \frac{\partial U(R, R_{0\,1/2})}{\partial R_{1/2}}\Big|_{R_{1/2}=R_{0\,1/2}}. \tag{49}$$

Assuming that $U(R)$ has the Woods–Saxon radial dependence, from (48) and (49) we obtain

$$U(R, R_{1/2}(E)) = U(R, R_{0\,1/2})[1 - \alpha(R) E];$$

$$\alpha(R) = (\gamma_R/a) \exp[(R - R_{0\,1/2})/a] / [1 + \exp((R - R_{0\,1/2})/a)].$$

TABLE IV. Real part of the OP for the system $\alpha + {}^{90}$Zr.

E_α, MeV	40	60	80	100	120	150	200	250	300
$-U_0$, MeV	241,7	238,6	235,6	232,7 128,9*	230,3	226,6	221,6	217,5	214,1
$-U$, MeV ($R = 6$ F)	48,65	47,57	46,54	45,58 48,14*	44,79	43,58	42,02	40,20	39,84

*Values of the potential for the Woods–Saxon parametrization for $E_\alpha = 104$ MeV.

It is easy to see that $\alpha(R_{1/2}) > \alpha(0)$ and that the maximum of the function $\alpha(R)$ is located in the surface region of the nucleus. These conclusions coincide with those obtained in the semimicroscopic analysis [see the discussion of Eq. (45) above].

3. SOME FEATURES OF THE MANIFESTATION OF THE NUCLEAR RAINBOW EFFECT

For a long time it was assumed that the analysis of elastic scattering of composite particles on nuclei can give only information on the behavior of the nucleus–nucleus potential in the vicinity of the strong-absorption radius.[1] This assumption was based on the concept of strong absorption in the surface region, which led to the conclusion that there is a discrete ambiguity in determining the OP parameters. Two phenomena, differing in their manifestations, were discovered in connection with the study of elastic scattering of α particles on nuclei and led to a review of these ideas. The phenomenon of so-called anomalous inverse scattering[47] of low-energy α particles on light ($A \leqslant 44$) nuclei with cluster structure showed that the scattering results are sensitive to the behavior of the potential in the interior of the nucleus and, in particular, to the presence of a core in the α-particle OP. The other phenomenon—the nuclear rainbow effect—appeared in the scattering of α particles of sufficiently high energy on both light and also intermediate and heavy nuclei; here no relation between this phenomenon and the cluster structure of the target nucleus was discerned.

The NR effect in α-particle scattering was first discovered in Refs. 5, 6, and 48 in the study of the interaction of α particles of energy $E_\alpha \simeq 140$ MeV with the nuclei ^{12}C, ^{40}Ca, ^{58}Ni, and ^{90}Zr. A characteristic feature of the NR effect is distortion, beginning at some scattering angle ($\theta_{\rm NR}$), of the diffraction pattern, the formation of a broad maximum in the angular distribution, and then exponential falloff of the scattering cross section. In the range of angles intermediate between the diffraction pattern and the maximum, the cross section is described by the Airy function,[49] and usually such behavior of the shape of the angular distribution is also related to the appearance of the NR effect.[50,51] According to the semiclassical analysis,[52] the nuclear rainbow scattering angle $\theta_{\rm NR}$ is related to the potential as

$$\theta_{\rm NR} \simeq \theta_{\rm CR} - 0{,}56\ (V/E)\ (R_v/a_v)^{1/2}, \qquad (50)$$

where $\theta_{\rm CR} = V_C/E$ is the Coulomb rainbow scattering angle and V_C is the Coulomb barrier. Equation (50) is valid for the Woods–Saxon parametrization of the radial dependence of the potential.

Equation (50) suggests that it is possible to eliminate the discrete ambiguity in the determination of the OP parameters in analyzing the α-particle angular distributions for angles $\theta > \theta_{\rm NR}$ (Refs. 6, 53, and 54). In Ref. 6 a unique family of optical α-particle potentials in the Woods–Saxon form was determined for each target nucleus. It was also found[6] that the angle $\theta_{\rm NR}$ depends roughly linearly on A.

In analyzing the NR effect in elastic scattering, wide use has been made of the decomposition of the scattering amplitude into "near," $f_N(\theta)$, and "far," $f_F(\theta)$, components, referred to as the N/F decomposition.[55,56] According to semiclassical ideas,[56] the near component of the amplitude $f_N(\theta)$ corresponds to scattering at the near (relative to the scattered particle) edge of the potential, while $f_F(\theta)$ corresponds to scattering at the far edge of the potential. The N/F decomposition permits the determination of the contribution to the scattering cross section from the far edge of the potential, i.e., from its interior. It becomes possible to test the potential at distances less than R_{SA}. We stress the fact that here we mean not the study of the potential at short distances, in general, but at distances inside the nucleus of $\Delta R = 1$–2 F from R_{SA}. In Fig. 8 we show the contribution to

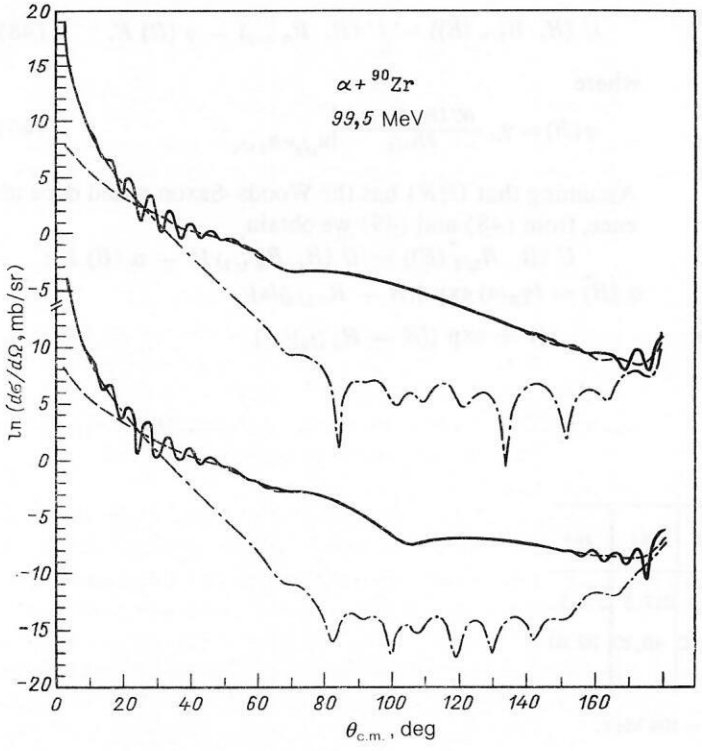

FIG. 8. Decomposition of the optical scattering amplitude for the system $\alpha + {}^{90}$Zr for $E_\alpha = 99.5$ MeV into near (dot–dash lines) and far (dashed lines) components; the solid lines are the coherent sum of the contributions of these components. The upper part of the figure is for the M3Y potential, and the lower part is for the M3Y (PP) potential.

the cross section for elastic scattering of α particles of energy 99.5 MeV on the ^{90}Zr nucleus from the near and far components of the amplitude calculated with the M3Y and M3Y (PP) potentials in Ref. 35. It can be seen that the contribution to the cross section from $f_F(\theta)$ dominates in both cases for $\theta > \theta_{NR}$.

Until recently, discovery of the NR effect in the scattering of heavy ions on nuclei was considered unlikely (see, for example, Refs. 56 and 58), owing to strong absorption and low transparency of the nuclear surface to heavy ions. However, in a recent study[59] the elastic scattering of ^{16}O ions on ^{16}O target nuclei at $E_{lab} = 350$ MeV was investigated. The authors noted that their results were the first to unambiguously indicate the manifestation of the NR effect in heavy-ion scattering ($A > 6$). The angular distributions were successfully described using the M3Y (PP) potential with the renormalization coefficient of the effective interaction $N = 1$ (Ref. 59). The ^{6}Li nucleus can be viewed as intermediate between light (^{3}He, ^{4}He) and heavy ($A > 6$) ions. The situation regarding the observation of the NR effect in ^{6}Li scattering is ambiguous. Rudimentary manifestations of the NR were observed in the scattering of ^{6}Li ions of energy $E = 93$ MeV on ^{13,14}C nuclei in Ref. 60, where it was not possible to uniquely determine the potential. Meanwhile, in Ref. 61 the interaction of ^{6}Li ions of energy $E = 210$ MeV with ^{28}Si, ^{40}Ca, ^{90}Zr, and ^{208}Pb nuclei was studied. The observed range of scattering angles was extended to include scattering angles corresponding to the NR. As a result, it proved possible to uniquely determine the potentials for ^{6}Li. The analysis carried out in Ref. 58 showed that the NR effect appears in the reaction ^{12}C(^{6}Li,^{6}Li) at $E = 90$ MeV, but is absent in the reaction ^{28}Si(^{6}Li,^{6}Li) at $E = 154$ MeV. Therefore, additional experimental studies are required to clear up the question of the NR phenomenon in the case of the scattering of heavy ions on nuclei.

The extension of the region of manifestation of NR effects in the interaction of composite particles with nuclei and, in particular, to inelastic processes has been discussed in Refs. 62 and 63. NR effects were first observed in charge-exchange processes in Ref. 64, where the angular distributions for the charge-exchange reaction ^{14}C(^{3}He,t)^{14}N with transition to the ground, analog, and Gamow–Teller states of the nucleus ^{14}N were studied in a wide angular range. The charge-exchange microscopic form factor was used in the analysis. The description of the effect turned out to be sensitive to both the behavior of the OP, and the form factor at distances smaller than R_{SA} ($R \sim 6$ F). In Ref. 65 it was also pointed out that it is necessary to use data on charge-exchange reactions to eliminate the ambiguities in the determination of the real part of the OP related to correlations between the real and imaginary parts of the OP. Therefore, the study of inelastic processes accompanied by manifestations of the NR effect can turn out to be a sensitive tool for studying the nucleus–nucleus interaction at distances smaller than R_{SA} (Ref. 64).

To conclude this section, let us discuss the general features of the theoretical approaches to describing scattering and, in particular, NR effects in scattering. There are two such approaches: the S-matrix approach and the potential approach. In the S-matrix approach the formalism of the description does not involve information on the properties of the nucleus–nucleus potential; the S-matrix elements are parametrized, and the corresponding parameters are extracted by comparing theory and experiment. The application of this approach to the description of the NR effect in scattering has been described in the recent review of Ref. 58, so that we shall not dwell on it here. We only note that by using an equation containing 13 parameters it was possible to successfully describe the angular distributions of ^{3}He and α particles scattered on a large group of nuclei for $E > 100$ MeV, and also the elastic scattering of ^{6}Li ions. In the potential approach the theoretical description is based on the explicit introduction of the nucleus–nucleus potential. This potential is either parametrized in the Woods–Saxon or a similar form, or is calculated on the basis of effective NN forces. Methods for this construction are discussed in the first few sections of this review. It seems preferable to use the potential approach for describing NR effects in scattering, since in this case it becomes possible to understand which factors—the nature of the effective NN forces, the inclusion of one-nucleon exchange effects, and so on—affect the behavior of the potential in the surface region and, therefore, the manifestation of NR effects.

4. ANALYSIS OF THE EXPERIMENTAL DATA

Let us study the application of the scheme for including one-nucleon exchange effects in the nucleus–nucleus interaction to the analysis of the experimental data on the scattering of composite particles on nuclei, including data in which NR effects are manifested. In order to be able to carry out a systematic and reliable analysis, it is necessary to have experimental data in wide energy and angular ranges. Analysis in a wide energy range makes it possible to test the theoretical predictions about changes in the potential geometry as a function of energy. These changes, as was shown above in Sec. 2, are related to the explicit inclusion of one-nucleon exchange effects. The use of an extended angular range makes it possible to apply the χ^2 minimization procedure and determine the parameters of the potential or the effective interaction more reliably. This statement is illustrated in Fig. 9, in which we show two variants of the calculation from Ref. 17 together with the experimental data from Ref. 66. The dashed line corresponds to the calculation with the M3Y (PP) potential, where to obtain the optimal description of the experimental angular distributions we have introduced the normalization factor $N_R = 0.55$. Both the cross section near θ_{NR} and the fine diffraction structure at very small angles are described qualitatively ($\chi^2/F \simeq 89$, where F is the number of degrees of freedom). The solid line corresponds to the computational scheme in which the fit with the M3Y (PP) potential is made only in the range of angles up to $\theta = 30°$, where $\chi^2/F = 3.0$, i.e., a very good fit with small renormalization of the interaction ($N_R = 0.96$) is obtained, but beyond the rainbow scattering angle the theoretical cross sections differ from the experimental ones by several orders of magnitude.

In Refs. 12, 13, and 35 the iterationless scheme for calculating one-nucleon exchange effects described above in Sec. 2 was used to analyze the following experimental data on elastic and inelastic scattering of composite particles on nuclei: ^{58}Ni(α,α) for $E = 104$ MeV (Ref. 67), 139 MeV (Ref. 48), and 172.5 MeV (Ref. 66); ^{58}Ni(α,α') for $E = 139$ MeV (Ref. 48); ^{90}Zr(α,α) for $E = 40$, 59.1, 79.5, 99.5, and 118 MeV (Ref. 36); ^{90}Zr(α,α') for $E = 99.5$ MeV (Ref. 36);

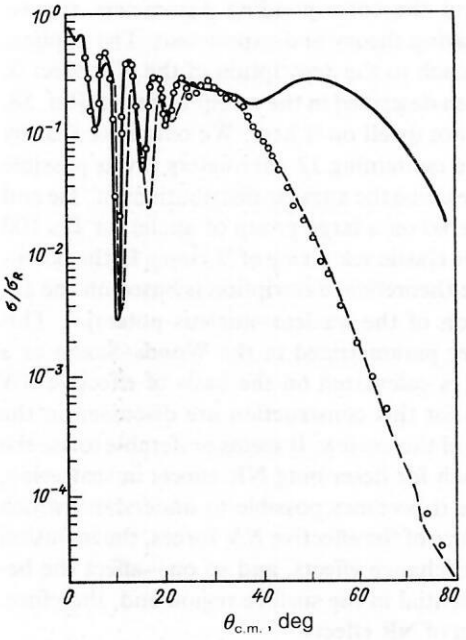

FIG. 9. Angular distributions of α particles scattered by ^{58}Ni for $E_\alpha = 172.5$ MeV: solid line—calculation with the M3Y (PP) potential and fit for the angular range $\theta < 30°$; dashed line—calculation with the renormalized M3Y (PP) potential. The points are the experimental data.

^{208}Pb(α,α) for $E = 27.6$ MeV (Ref. 68), 42 MeV (Ref. 69), 104 MeV (Ref. 70), 139 MeV (Ref. 48), and 166 MeV (Ref. 71); ^{12}C(α,α) for $E = 139$ MeV (Ref. 72); ^{40}Ca(α,α) for $E = 104$ MeV (Ref. 73); ^{12}C(^{6}Li,^{6}Li) and ^{40}Ca(^{6}Li,^{6}Li) for $E = 156$ MeV (Ref. 74); ^{12}C(^{9}Be,^{9}Be) for $E = 158.3$ MeV and ^{16}O(^{9}Be,^{9}Be) for $E = 157.7$ MeV (Ref. 75); ^{208}Pb(^{16}O,^{16}O) in the range $78 \leqslant E \leqslant 312.6$ MeV; ^{208}Pb(^{16}O,^{16}O) for $E = 104$ MeV (Refs. 76–79); ^{40}Ca(^{16}O,^{16}O) in the range $40 \leqslant E \leqslant 214.1$ MeV (Refs. 80–82); ^{40}Ca(^{40}Ca,^{40}Ca) in the range $129.6 \leqslant E \leqslant 240.0$ MeV (Ref. 83).

Since the M3Y and M3Y (PP) effective interactions are real, imaginary potentials from the standard optical model are added to the real M3Y and M3Y (PP) potentials, and the absorption potential is taken in the Woods–Saxon form. The parameters $\beta_L^{(I)}$ are extracted from the expression (see Ref. 1) $\beta_L^{(I)} R_v = \beta_L^{(c)} R_{Ch}$, where the charge radii are found from the data on electron scattering,[84] and the charge-distribution deformation parameters are extracted from the measured values of the electromagnetic transition probabilities $B(EL)$.

The densities $\rho(r)$ for the α particle and ^{6}Li were taken to have the form of Gaussians with parameters from Refs. 2 and 85, respectively; for ^{9}Be, $\rho(r)$ is calculated using the independent-particle model (version B) (Ref. 86). The two-parameter Fermi distributions with parameters from Ref. 19 are taken as $\rho(r)$ for ^{12}C, ^{16}O, and ^{40}Ca. The densities $\rho(r)$ and transition densities $\rho_\lambda(r)$ for intermediate and heavy target nuclei are calculated using the QPM (Ref. 87).

The results of the analysis of the elastic and inelastic scattering of α particles are given in Figs. 10–14 and Tables V–VII. The α-particle energies, equal to 139 and 172.5 MeV in the case of ^{58}Ni, are sufficient for NR effects to appear (Fig. 10). In Ref. 38 it was shown that in the scattering of α particles with $E = 139$ MeV the real part of the OP is uniquely determined in the form $(WS)^2$ and has a depth of about 140 MeV. We see that the M3Y (PP) potentials give a poor description of the data for both elastic and inelastic scattering (Figs. 10 and 12). In the case of elastic scattering this disagreement is related to the fact that the M3Y (PP) potentials are too deep in the interior region. After renormalization with $N_R = 0.7$ they become shallower than the M3Y potentials in the surface region, and therefore they do not lead to the correct description of the oscillations for forward angles. The explicit inclusion of one-nucleon exchange effects (the use of M3Y potentials) gives a good description of the angular distributions of both elastically and inelastically scattered α particles in the entire angular range.

In Figs. 11 and 13 we show the results of the analysis of elastic scattering of α particles on ^{90}Zr in a wide energy range and also of inelastic scattering for $E = 99.5$ MeV. As the energy increases the difference in the quality of the description of the experimental angular distributions using the M3Y (PP) and M3Y potentials grows. For example, for

TABLE V. Optical potentials for the scattering of α particles on the nuclei ^{12}C, ^{40}Ca, ^{58}Ni, and ^{90}Zr.

Nucleus	E_{lab}, MeV	V_{eff}	N_R	$-U_0$, MeV	J_R, MeV·F^3	$\langle r^2\rangle^{1/2}$, F	$-W_v$, MeV	r_v, F	a_v, F	χ^2/F
^{12}C	139	M3Y (PP)	0,722	123,2	270,5	3,201	19,72	1,568	0,634	31,7
		M3Y	0,731	124,1	278,2	3,264	19,93	1,517	0,775	9,4
^{40}Ca	104	M3Y (PP)	0,696	163,2	269,0	4,053	26,94	1,342	0,853	80,8
		M3Y	0,739	156,3	294,8	4,157	23,65	1,478	0,766	13,5
^{58}Ni	139	M3Y (PP)	0,695	146,7	250,0	4,424	25,48	1,382	0,864	49,9
		M3Y	0,785	139,7	277,7	4,524	23,62	1,473	0,775	6,1
^{58}Ni	172,5	M3Y (PP)	0,670	137,1	243,3	4,434	22,24	1,429	0,900	25,2
		M3Y	0,780	132,1	262,4	4,538	22,31	1,483	0,816	4,9
^{90}Zr	40	M3Y (PP)	1,134	282,7	463,0	4,830	17,63	1,472	0,614	26,2
		M3Y	1,157	261,5	476,4	4,921	21,92	1,400	0,575	10,9
^{90}Zr	59,1	M3Y (PP)	1,377	337,3	553,6	4,834	23,48	1,554	0,479	14,1
		M3Y	0,986	215,3	392,9	4,931	26,58	1,293	0,907	9,6
^{90}Zr	79,5	M3Y (PP)	0,972	233,9	383,8	4,839	23,23	1,463	0,728	16,9
		M3Y	0,777	163,9	299,3	4,940	21,66	1,447	0,775	13,6
^{90}Zr	99,5	M3Y (PP)	0,987	233,3	382,9	4,844	27,28	1,437	0,766	29,6
		M3Y	0,780	159,1	291,0	4,949	26,23	1,384	0,907	13,3
^{90}Zr	118	M3Y (PP)	0,686	159,5	261,7	4,849	26,31	1,351	0,909	33,6
		M3Y	0,779	154,6	282,2	4,956	22,77	1,470	0,747	7,0

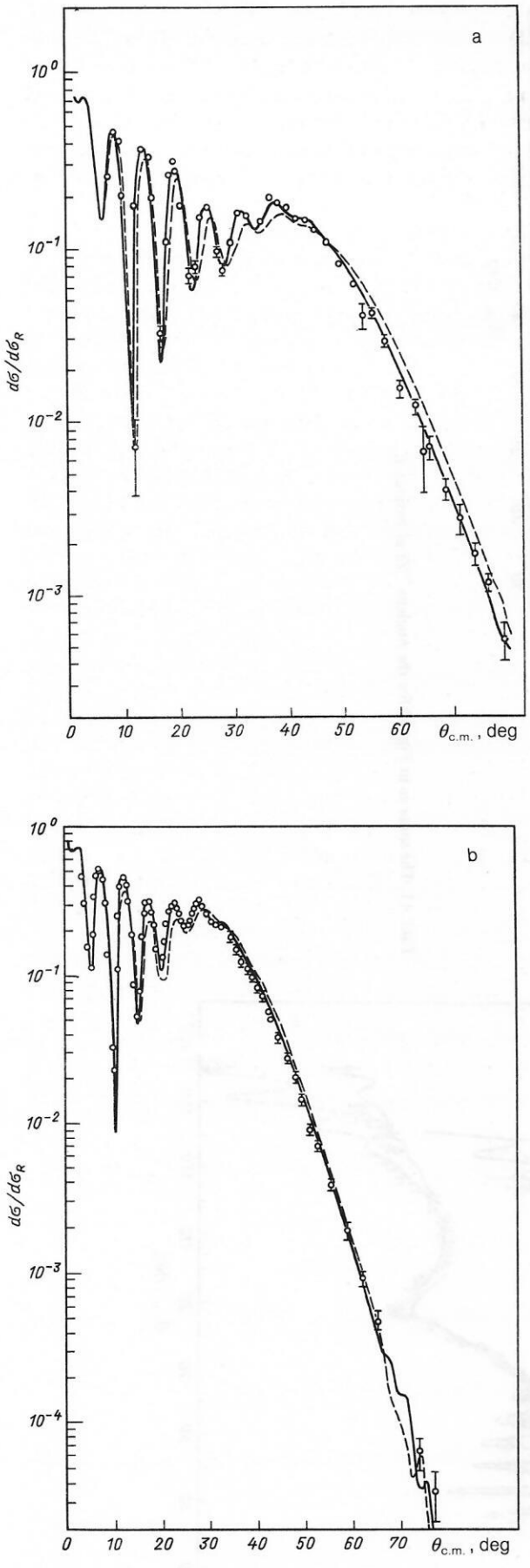

FIG. 10. Angular distributions of α particles scattered by ^{58}Ni for $E_\alpha = 139$ MeV (a) and $E_\alpha = 172.5$ MeV (b): the solid lines are the calculation with the M3Y potential, the dashed lines are for the M3Y (PP) potential, and the points are the experimental data.

$E = 99.5$ MeV the pseudopotential approximation does not describe the broad maximum for $\theta > \theta_{NR}$ typical of the NR effect, while when one-nucleon exchange effects are included explicitly all the characteristic features of the NR are described. This is consistent with the fact that the M3Y potential is very close to the OP extracted from the MIA in the range $3 \leqslant R \leqslant 8$ F (see Fig. 4), and it is in this range that there are significant differences between the M3Y and M3Y (PP) potentials. The decomposition of the scattering amplitude into far and near components (Fig. 8) illustrates the statement that the dominant contribution in the NR region and up to angles $\theta \sim 150°$ comes from the far component of the amplitude, i.e., refraction on the interior part of the potential. We note that the analysis carried out earlier for this case[36] using the simple folding model also leads to disagreement between the theoretical predictions and the experimental data. A successful fit was achieved only by modifying the density $\rho(r)$ in ^{90}Zr, which had no physical justification.

In Table VI we give the data from a comparative analysis of various methods of describing the elastic scattering of α particles with energies from 40 to 118.0 MeV on the nucleus ^{90}Zr. We see that the six-parameter optical model gives the best description of the experimental data (if the criterion of minimum χ^2 is used). Potentials with fixed geometry in the optical model lead to a considerably worse description of the angular distributions at low energies. Analysis of the microscopic potentials (see columns 4–6 of Table VI) shows that increasingly accurate inclusion of one-nucleon exchange effects (progression to the pseudopotential approximation, and from it to the density-matrix formalism) leads to systematic decrease of the quantity χ^2/F. Regarding the global comparison (see the last line in Table VI) of the microscopic potentials and the phenomenological potentials, the simple folding model gives just as good a description as the optical model with fixed geometry, and the M3Y potentials describe the experimental data just as well as the six-parameter optical model.

The cross sections for inelastic scattering with excitation of the states $|2_1^+\rangle$ and $|3_1^-\rangle$ in the target nucleus, shown in Figs. 12 and 13, were calculated with the transition densities constructed in the QPM assuming the one-phonon nature of these states. The calculation was carried out in both the DWA and the CCM (coupled-channel method). The differences turned out to be insignificant.[21] The discrepancies related to the inclusion of one-nucleon exchange effects in the distorting OP are more important. The pseudopotential approximation does not reproduce the oscillations in the cross sections for the inelastic scattering of α particles on ^{58}Ni at forward angles, and also the angular distributions for $\theta > 70°$ for the scattering of α particles on ^{90}Zr, while the M3Y potentials reproduce the inelastic scattering cross sections well, except at very small angles ($\theta < 5°$) for ^{90}Zr.

The interaction of α particles with energies from 27.6 to 166 MeV with the target nucleus ^{208}Pb was also analyzed in Ref. 12. Whereas at low energies the M3Y (PP) potentials in this case were shallower than the M3Y potentials both in the interior region and at the nuclear surface, at high energies ($E > 100$ MeV) the M3Y (PP) potentials turned out to be deeper in the interior region, remaining shallower than the M3Y potentials at the surface. Therefore, again in the case of the nucleus ^{208}Pb the inclusion of one-nucleon exchange effects leads to change of the potential geometry with increas-

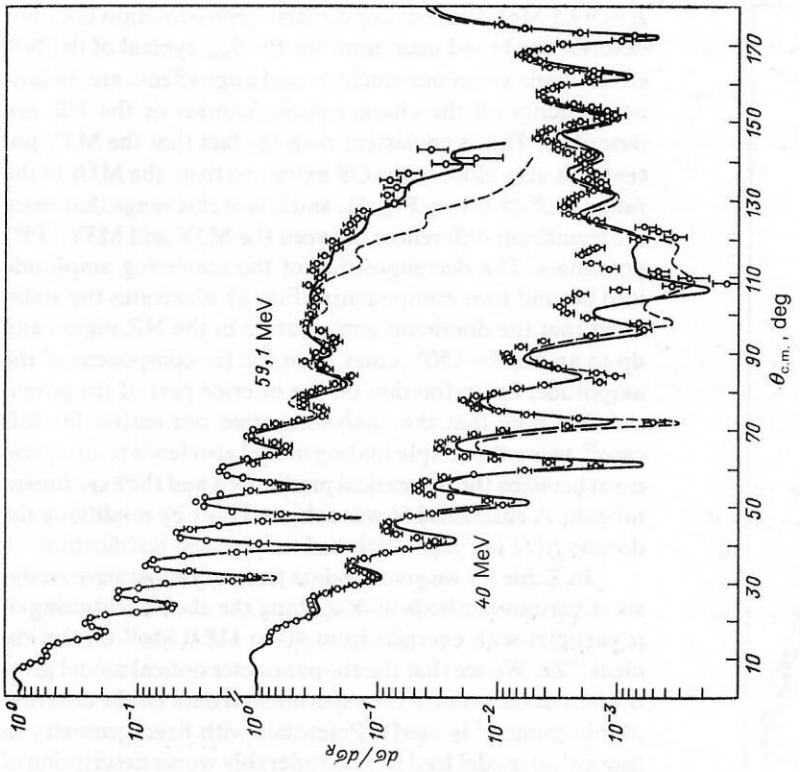

FIG. 11. The same as in Fig. 10 for the nucleus ^{90}Zr at various E_α.

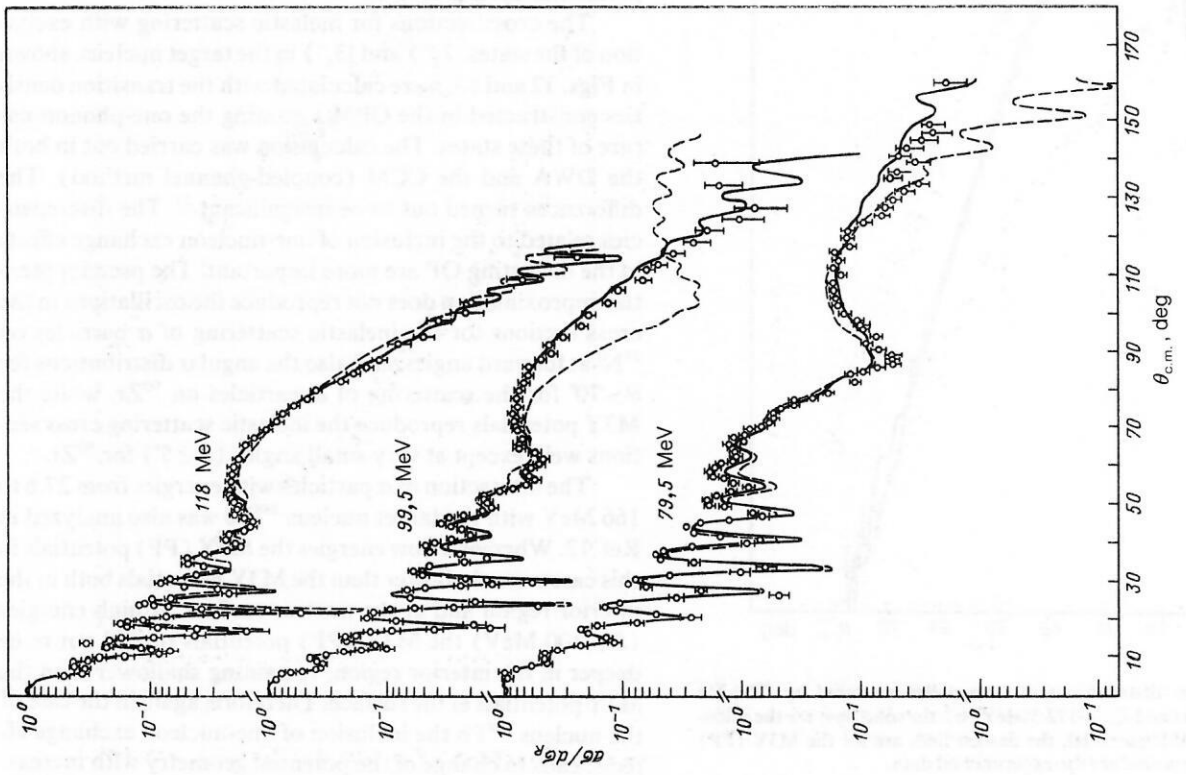

TABLE VI. χ^2/F in different variants of the analysis of elastic scattering of α particles on ^{90}Zr.

E_α, MeV	Variant of the analysis				
	I	II	III	IV	V
40,0	6	82,6	34,1	26,2	10,9
59,1	14,9	28,5	23,3	14,1	9,6
79,5	9,2	9,6	21,7	16,9	13,6
99,5	5,1	6,0	32,7	29,6	13,3
118,0	5,2	5,1	25,0	33,6	7,0
$\sum_{E_\alpha} \chi^2/F$	40,4	131,8	136,8	120,4	54,4

Note. (I) Six-parameter optical model (Ref. 36); (II) optical model with fixed "geometry" (Ref. 36); (III) folding model with $\lambda(E)$ (Ref. 36); (IV) M3Y (PP) potentials for the real part of the OP (Ref. 12); (V) M3Y potentials for the real part of the OP (Ref. 35).

ing energy. The results of the analysis of the angular distributions of elastically scattered α particles for three values of the energy are given in Table VII. These experimental data were mainly obtained at forward scattering angles,[48,70,71] so that their descriptions by the M3Y (PP) and M3Y potentials turned out to be of similar quality (see χ^2/F in Table VII). The entire difference reduced to the values of the normalization factor N_R.

In relation to the presence of definite cluster features in the target nuclei ^{12}C and ^{40}Ca, it is of particular interest to analyze α-particle interactions with these nuclei in the den-

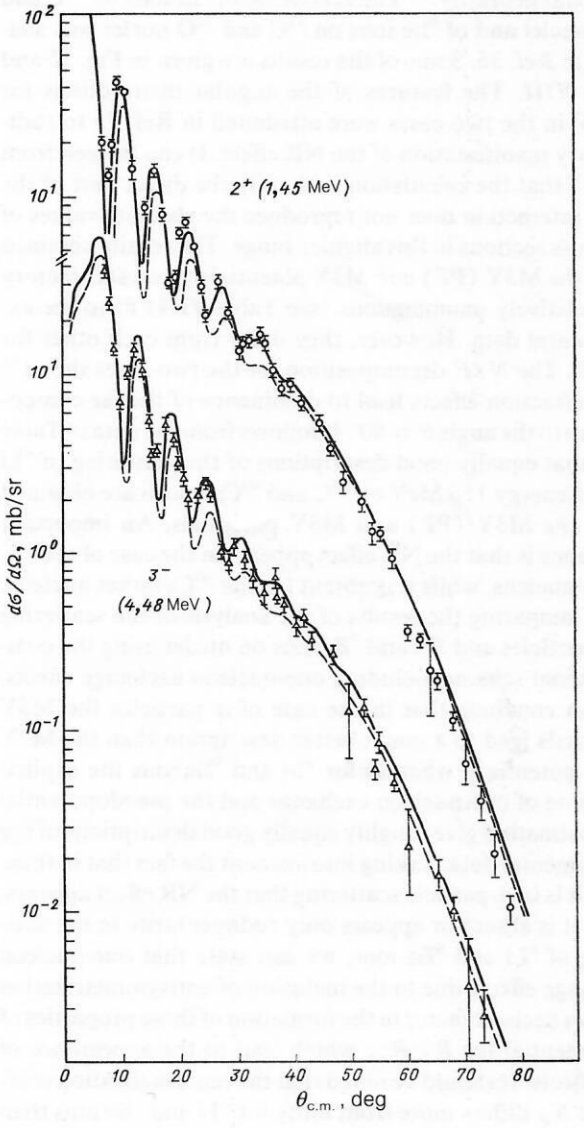

FIG. 12. Inelastic scattering cross sections for $\alpha + {}^{58}$Ni for $E_\alpha = 139$ MeV. The solid lines are the calculation with the M3Y potentials and form factors, the dashed lines are the calculations with the M3Y (PP) potentials, and the points are the experimental data.

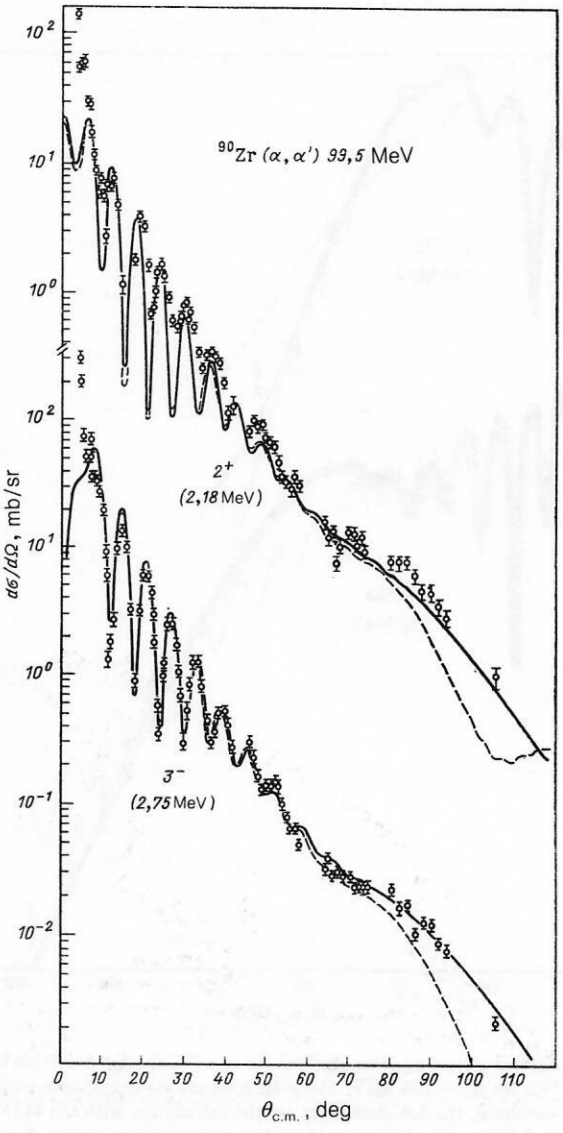

FIG. 13. The same as in Fig. 12 for $\alpha + {}^{90}$Zr for $E_\alpha = 99.5$ MeV.

TABLE VII. Optical potentials for the scattering of α particles on the nucleus ^{208}Pb.

E_{lab}, MeV	V_{eff}	N_R	$-U_0$, MeV	J_R, MeV·F^3	$\langle r^2\rangle^{1/2}$, F	$-W_v$, MeV	r_v, F	a_v, F	χ^2/F
104,0	M3Y (PP)	1,016	244,5	392,7	6,008	23,54	1,461	0,694	7,5
	M3Y	0,839	189,0	330,5	6,137	28,10	1,428	0,719	7,2
139,0	M3Y (PP)	1,126	262,5	421,7	6,015	23,09	1,475	0,755	13,8
	M3Y	0,972	204,9	359,3	6,149	22,74	1,470	0,795	10,9
166,0	M3Y (PP)	0,904	205,2	329,9	6,021	23,64	1,428	0,849	18,9
	M3Y	0,756	151,9	266,5	6,159	20,35	1,442	0,924	16,2

sity-matrix formalism. In Fig. 14 and Table V we give the results of the description of the elastic scattering of α particles of energy 139 MeV on ^{12}C nuclei and of energy 104 MeV on ^{40}Ca nuclei. It can be seen that the use of only the direct part of the M3Y interaction [see Eq. (1)] in the analysis without one-nucleon exchange effects leads to a poor description of the data (the absolute values of the cross sections are not reproduced) in the entire angular range, except at very small angles. It follows from Table V that the M3Y potentials give a considerably better description of the angular distributions than the M3Y (PP) potentials. The successful description of α-particle scattering on light nuclei indicates that one-nucleon exchange effects apparently exhaust the contribution of exchange correlations for light target nuclei to the α-particle potential at sufficiently high energies. This statement is also consistent with the conclusion, drawn on the basis of an analysis using the resonating-group method, that one-nucleon exchange dominates at high energies.[25]

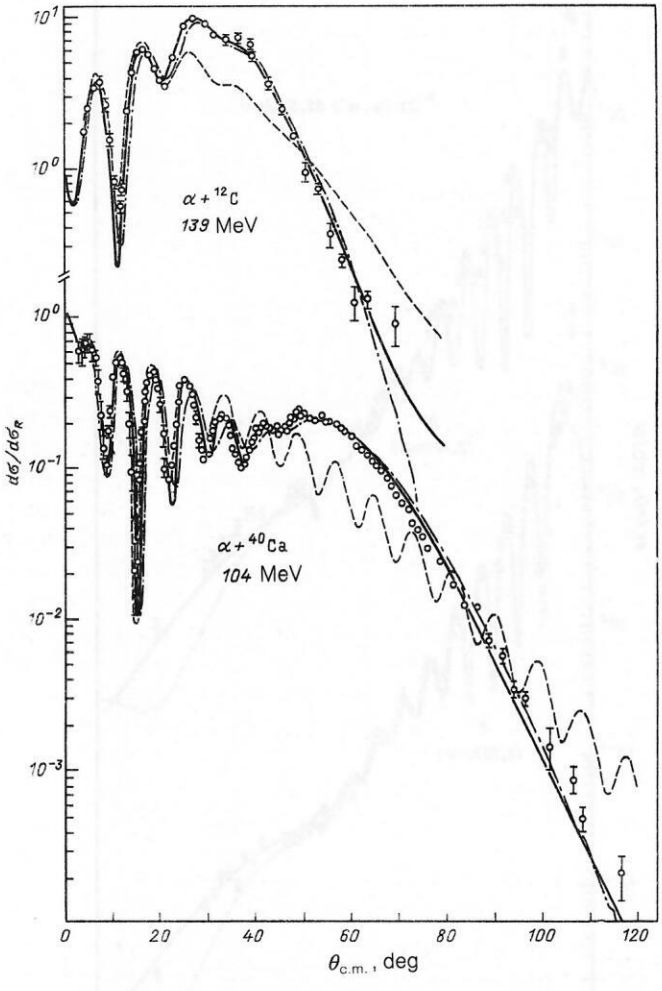

FIG. 14. Elastic scattering cross sections for $\alpha + ^{12}$C for $E_\alpha = 139$ MeV and $\alpha + ^{40}$Ca for $E_\alpha = 104$ MeV. The solid lines are the calculation with the M3Y potential, the dot–dash lines are the calculation with the M3Y (PP) potential, the dashed lines are the calculation with the "direct" part of the M3Y interaction, and the points are the experimental data.

As we noted above, for ions heavier than α particles, the NR effect does not appear in the scattering, or it appears only rudimentarily.[75] The scattering of ^{6}Li ions on ^{12}C and ^{40}Ca nuclei and of ^{9}Be ions on ^{12}C and ^{16}O nuclei was analyzed in Ref. 36. Some of the results are given in Fig. 15 and Table VIII. The features of the angular distributions for $\theta > 45°$ in the two cases were attributed in Ref. 75 to rudimentary manifestation of the NR effect. It can be seen from Fig. 15 that the calculation with only the direct part of the M3Y interaction does not reproduce the absolute values of the cross sections in this angular range. The results obtained using the M3Y (PP) and M3Y potentials give a satisfactory and relatively unambiguous (see Table VIII) fit to the experimental data. However, they differ from each other for $\theta > 55°$. The N/F decomposition for the two cases shows[35] that refraction effects lead to dominance of the far component up to the angle $\theta = 80°$. It follows from the data of Table VIII that equally good descriptions of the scattering of ^{6}Li ions of energy 156 MeV on ^{12}C and ^{40}Ca nuclei are obtained using the M3Y (PP) and M3Y potentials. An important difference is that the NR effect appears in the case of the ^{12}C target nucleus, while it is absent for the ^{40}Ca target nucleus.

Comparing the results of the analysis of the scattering of α particles and ^{6}Li and ^{9}Be ions on nuclei using the computational scheme including one-nucleon exchange effects, we can conclude that in the case of α particles the M3Y potentials lead to a much better description than the M3Y (PP) potentials, whereas for ^{6}Li and ^{9}Be ions the explicit inclusion of one-nucleon exchange and the pseudopotential approximation give roughly equally good descriptions of the experimental data. Taking into account the fact that in these cases it is in α-particle scattering that the NR effect appears, while it is absent or appears only rudimentarily in the scattering of ^{6}Li and ^{9}Be ions, we can state that one-nucleon exchange effects due to the inclusion of antisymmetrization is also a decisive factor in the formation of those properties of the potential for $R < R_{SA}$ which lead to the appearance of NR effects. It should be noted that the renormalization coefficient N_R differs more from unity for ^{6}Li and ^{9}Be ions than in the case of α particles (cf. the data in Tables V, VII, and VIII). This can be related to the fact that for such weakly coupled systems as ^{6}Li and ^{9}Be, breakup processes or cluster

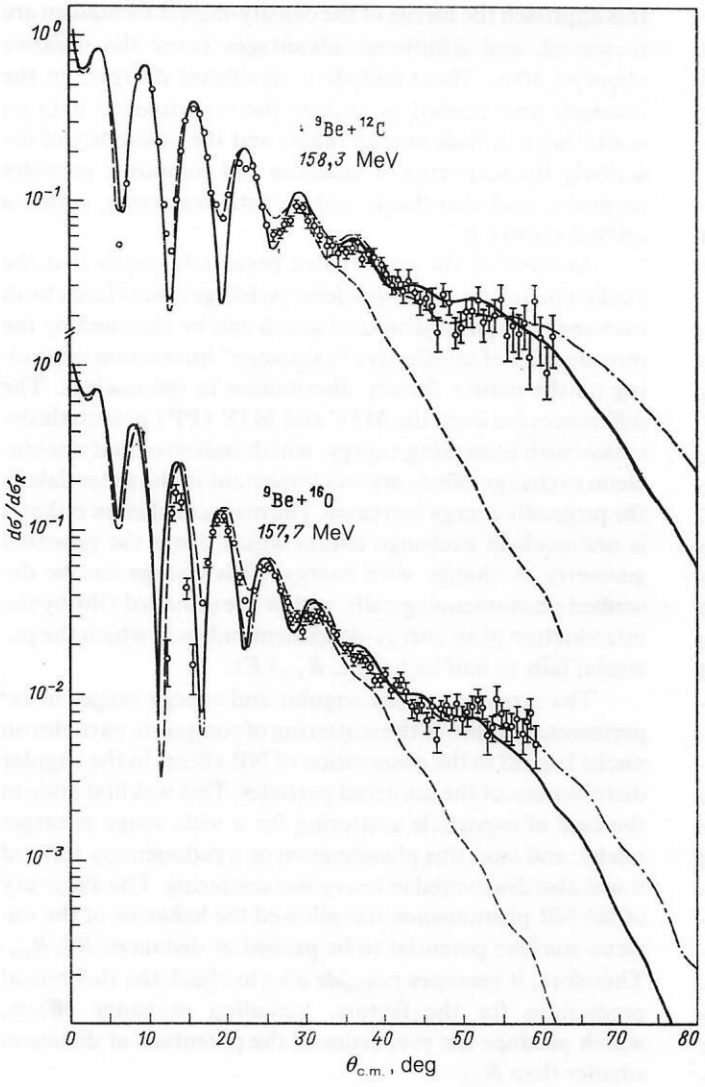

FIG. 15. The same as in Fig. 14 for $^9Be + ^{12}C$ for $E = 158.3$ MeV and $^9Be + ^{16}O$ for $E = 157.7$ MeV.

exchange effects can be important.[88,89] Moreover, the calculations of Ref. 35 did not include the spin–orbit interaction and the effect of nuclear deformation (^9Be has quadrupole moment $Q_2 = 5.3$ F^2) on elastic scattering. Although these effects are not negligible, they do not introduce important changes in the central potential.[74,90]

It follows from the scheme described above for analyzing the experimental data in the density-matrix formalism that the only free parameter in the calculation of the real part of the OP is the renormalization parameter N_R (the parameter λ in Ref. 10). The introduction of the parameter cannot, however, compensate for the failure to explicitly include one-nucleon exchange effects in the pseudopotential approximation. In fact, as was shown in Sec. 2, these effects lead to a change of the potential geometry with increasing energy. This change cannot be obtained by a scale transformation (even an energy-dependent one) of the M3Y (PP) potential. We note that when one-nucleon exchange effects are explicitly included, i.e., when using the terminology of Refs. 9–11, antisymmetrization effects are treated on the basis of first principles, the coefficients N_R (or λ) are the same for α particles and heavy ions (see Tables V, VII, VIII, and Table

TABLE VIII. Optical potentials for the scattering of ^6Li and ^9Be ions.

System	E_{lab}, MeV	V_{eff}	N_R	$-U_0$, MeV	J_R, MeV·F^3	$\langle r^2\rangle^{1/2}$, F	$-W_v$, MeV	r_v, F	a_v, F	χ^2/F
$^6Li + ^{12}C$	156	M3Y (PP)	0,793	147,4	306,5	3,711	44,74	1,486	0,837	8,8
		M3Y	0,642	132,8	298,7	3,786	52,89	1,302	0,972	7,8
$^6Li + ^{40}Ca$	156	M3Y (PP)	0,713	211,3	275,3	4,478	32,41	1,653	0,924	6,8
		M3Y	0,599	177,9	266,3	4,592	33,80	1,639	0,938	8,9
$^9Be + ^{12}C$	158,3	M3Y (PP)	0,812	203,0	323,1	3,837	30,88	1,032	0,929	20,2
		M3Y	0,706	203,2	312,9	3,887	31,99	1,029	0,923	18,1
$^9Be + ^{16}O$	157,7	M3Y (PP)	0,706	202,6	281,0	4,008	30,22	1,041	0,937	8,7
		M3Y	0,643	211,3	287,7	4,064	33,46	1,031	0,936	8,8

3 of Ref. 12). Therefore, a consistent description of the scattering of α particles and heavy ions on nuclei is obtained in this approach, while in the semiphenomenological model with the DDM3Y effective interaction the renormalization coefficients for α particles and heavy ions differ by more than a factor of 1.5 (they are 1.3 and 0.8, respectively). Whereas in the model with the DDM3Y interaction λ is independent of the energy, in the present approach N_R at low energies close to the Coulomb barrier is about unity, and at high energies it is about 0.8.

There are several factors causing N_R in this approach to differ from unity and causing the normalization factor to depend on the energy. First of all, there is the absence of any dependence of the M3Y effective interaction on $\rho(\mathbf{r})$. In Ref. 9, as was noted in Sec. 1 of this review, it was shown that the inclusion of one-nucleon exchange effects is equivalent to the inclusion of the density dependence in the exchange effective interaction. This type of dependence was referred to in Ref. 9 as the internal density dependence. In Ref. 19 it was noticed that in the Bruckner theory a dependence on $\rho(\mathbf{r})$ also arises in the direct term in the effective interaction. The isolation of this extra density dependence is a complicated theoretical problem. However, the use of the DDM3Y interaction in the density-matrix formalism would not be consistent, since the DDM3Y effective interaction already includes exchange effects in an approximate form. We can proceed by the route of introducing the density dependence in the parametrized form directly in Eq. (6). This method of constructing the α-particle potential, but with more approximate inclusion of exchange effects, was successfully realized in a unified description of elastic and inelastic scattering of low-energy nucleons and α particles on nuclei in Refs. 39 and 91. Another factor causing N_R to differ from unity might be the neglect of terms of second order in the effective NN forces in the calculation of the nucleus–nucleus potential. These terms describe the contribution to the potential from effects of going beyond the "frozen"-nucleon approximation. This approximation is typical of both the semimicroscopic approach and the semiphenomenological model of including exchange effects in the DDM3Y interaction. However, for internuclear distances of less than R_{SA} in a collision the densities of the colliding nuclei overlap significantly, so that in this case terms of second order in the effective NN forces in the potential can be important. It is laborious to calculate these effects (see the above discussion of the problem of calculating the absorption potential). Finally, n-nucleon ($n > 1$) exchange effects might have some influence on N_R.

CONCLUSION

In the density-matrix formalism the inclusion of one-nucleon exchange effects in the construction of nucleus–nucleus potentials is based on "first principles," i.e., explicit consideration of the density matrix $\rho(\mathbf{r},\mathbf{r}')$, for which the modified Slater approximation including surface effects is usually used. There are two methods of constructing nucleus–nucleus potentials with the introduction of $\rho(\mathbf{r},\mathbf{r}')$. The first is based on the use of an awkward iteration procedure in the calculation of the localized form of the exchange term in the potential. The second involves the use of an iterationless scheme for calculating the exchange potentials. In this approach the merits of the density-matrix formalism are preserved, and additional advantages (over the iterative scheme) arise. These include a significant decrease in the machine time needed to analyze the experimental data on scattering in a wide energy range, and the possibility of describing the scattering of nucleons and composite particles on nuclei, and also elastic and inelastic scattering, within a unified approach.

Analysis of the constructed potentials shows that the explicit inclusion of one-nucleon exchange effects leads to an exchange-potential structure which can be obtained by the introduction of an effective "exchange" interaction depending on the matter density distribution in the nucleus. The differences between the M3Y and M3Y (PP) potentials decrease with increasing energy, which indicates that one-nucleon exchange effects are less important in the potentials as the projectile energy increases. The main conclusion is that it is one-nucleon exchange effects which cause the potential geometry to change with energy. This change can be described phenomenologically within the standard OM by the introduction of an energy-dependent radius at which the potential falls to half its height, $R_{1/2}(E)$.

The extension of the angular and energy ranges in experimental studies of the scattering of composite particles on nuclei has led to the observation of NR effects in the angular distributions of the scattered particles. This was first done in the case of α-particle scattering for a wide range of target nuclei, and later this phenomenon or a rudimentary form of it was also discovered in heavy-ion scattering. The discovery of the NR phenomenon has allowed the behavior of the nucleus–nucleus potential to be probed at distances $R < R_{SA}$. Therefore, it becomes possible also to check the theoretical predictions for the factors, including exchange effects, which produce the properties of the potentials at distances smaller than R_{SA}.

The M3Y (PP) and M3Y potentials have been used to analyze the elastic (and in some cases inelastic) scattering of α particles, ^{6}Li and ^{9}Be ions, and also heavier ions on a group of target nuclei in a wide energy range. It has been shown that in those cases where the experimental data for α-particle scattering were obtained for an angular range sufficiently wide to observe the NR phenomenon, the M3Y (PP) and M3Y potentials lead to rather different descriptions of the experimental data, and a better description of the angular distributions is obtained when the M3Y potentials are used. However, in the case of a restricted angular range for α-particle scattering or in the description of the scattering of ^{6}Li and ^{9}Be ions and also heavier ions on nuclei the experimental data are described equally well when the M3Y and the M3Y (PP) potentials are used. Therefore, a crucial factor in reproducing NR effects in α-particle scattering is the inclusion of one-nucleon exchange in the construction of the α-particle OP. We have confirmed the earlier conclusion that the pseudopotential approximation is a good approximation for describing exchange effects in the interaction of heavy ions with nuclei. The successful description in the density-matrix formalism of the elastic scattering of α particles with energy $E_\alpha > 100$ MeV on ^{12}C and ^{40}Ca nuclei showed that one-nucleon exchange at sufficiently high energies exhausts the contribution of exchange effects to the α-particle potential. A better description of the elastic and inelastic (with excitation of low-lying states of the target

nucleus) scattering of α particles on ^{58}Ni and ^{90}Zr nuclei is obtained within the unified scheme. In contrast to the semiphenomenological inclusion of exchange effects in the double-convolution model with the DDM3Y interaction, in this approach a consistent description of the scattering of α particles and heavy ions on nuclei is obtained for the same values of the parameter describing the renormalization of the effective interaction, but these values display some energy dependence.

Let us discuss the possibilities for further study of the questions considered in this review. From the viewpoint of experimental studies, it is important to extend the angular and energy ranges in the scattering of semiheavy and heavy ions on nuclei in order to clarify the situation with regard to full or rudimentary manifestation of NR effects in these cases. It is also important to obtain data on quasielastic and inelastic processes. Such data can prove crucial for eliminating the discrete ambiguity in the determination of the potential in the region lying inside the strong-absorption sphere.

From the theoretical viewpoint it is necessary to extend the formalism to include not only nucleon–nucleon exchange correlations, but also multiparticle correlations modeled by the density dependence of the effective forces. It is also important to go beyond the "frozen"-nucleon approximation and include in the construction of nucleus–nucleus potentials terms of second order in the effective *NN* interaction, and to calculate the absorption potentials on a semimicroscopic basis. Finally, for a consistent description of elastic and quasielastic processes it is necessary to develop a computational scheme in which exchange effects in elastic and charge-exchange channels are taken into account in a unified manner.

In conclusion, the authors consider it their pleasant duty to thank F. A. Gareev, V. Z. Gol'dberg, S. G. Kadmenskiĭ, A. A. Ogloblin, and H. Rebel for useful discussions about the questions considered in this review.

[1)] Henceforth, for brevity the potentials constructed by the first method will be referred to as M3Y potentials, and those constructed by the second method will be referred to as M3Y (PP) potentials.

[1] G. R. Satchler, *Direct Nuclear Reactions* (Oxford University Press, New York, 1983).
[2] G. R. Satchler and W. G. Love, Phys. Rep. **55**, 183 (1979).
[3] Z. Majka, H. J. Gils, and H. Rebel, Z. Phys. A **288**, 139 (1978).
[4] F. Duggan, M. Lassaut, F. Michel *et al.*, Nucl. Phys. **A355**, 141 (1981).
[5] D. A. Goldberg and S. M. Smith, Phys. Rev. Lett. **29**, 500 (1972).
[6] D. A. Goldberg, S. M. Smith, and G. F. Burdzik, Phys. Rev. C **10**, 1362 (1974).
[7] K. Wildermuth and Y. C. Tang, *A Unified Theory of the Nucleus* (Academic Press, New York, 1977) [Russ. transl., Mir, Moscow, 1980].
[8] B. C. Sinha, Phys. Rep. **20**, 1 (1975).
[9] S. K. Gupta and B. Sinha, Phys. Rev. C **30**, 1093 (1984).
[10] A. K. Chaudhuri, D. N. Basu, and B. Sinha, Nucl. Phys. **A439**, 415 (1985).
[11] A. K. Chaudhuri and B. Sinha, Nucl. Phys. **A455**, 169 (1986).
[12] Dao Tien Khoa and O. M. Knyazkov, Z. Phys. A **328**, 67 (1987).
[13] Dao Tien Khoa and O. M. Knyaz'kov, Yad. Fiz. **47**, 1246 (1988) [Sov. J. Nucl. Phys. **47**, 793 (1988)].
[14] F. Petrovich, H. McManus, V. A. Madsen *et al.*, Phys. Rev. Lett. **22**, 895 (1969).
[15] G. Bertsch, J. Borysowicz, H. McManus *et al.*, Nucl. Phys. **A284**, 399 (1977).
[16] N. Anantaraman, H. Toki, and G. F. Bertsch, Nucl. Phys. **A398**, 269 (1983).
[17] A. M. Kobos, B. A. Brown, P. E. Hodgson *et al.*, Nucl. Phys. **A384**, 65 (1982); A. M. Kobos, B. A. Brown, R. Lindsay *et al.*, Nucl. Phys. **A425**, 205 (1984).
[18] J. P. Jeukenne, A. Lejeune, and C. Mahaux, Phys. Rev. C **16**, 80 (1977).
[19] M. Farid El-Azab and G. R. Satchler, Nucl. Phys. **A438**, 525 (1985).
[20] Y. Eisen and B. Day, Phys. Lett. **63B**, 253 (1976).
[21] B. Sinha and S. A. Moszkowski, Phys. Lett. **81B**, 289 (1979).
[22] B. Z. Georgiev and R. S. Mackintosh, Nucl. Phys. **A307**, 377 (1978).
[23] X. Campi and A. Bouyssy, Phys. Lett. **73B**, 263 (1978).
[24] J. W. Negele and D. Vautherin, Phys. Rev. C **5**, 1472 (1972).
[25] M. LeMere and Y. C. Tang, Phys. Rev. C **39**, 1696 (1989).
[26] T. Wada and H. Horiuchi, Prog. Theor. Phys. **80**, 502 (1988).
[27] J. S. McCarthy, L. Sick, and R. R. Whitney, Phys. Rev. C **15**, 1396 (1977).
[28] H. J. Gils, Nucl. Phys. **A473**, 111 (1987).
[29] T. Tamura, Rev. Mod. Phys. **37**, 676 (1965).
[30] O. M. Knyaz'kov and A. A. Nekrasov, Yad. Fiz. **38**, 36 (1983) [Sov. J. Nucl. Phys. **38**, 20 (1983)].
[31] I. S. Gradshteyn and I. M. Ryzhik, *Tables of Integrals, Series, and Products*, transl. of the 4th Russ. ed. (Academic Press, New York, 1980) [Russ. original, Fizmatgiz, Moscow, 1963].
[32] O. M. Knyaz'kov, Fiz. Elem. Chastits At. Yadra **17**, 318 (1986) [Sov. J. Part. Nucl. **17**, 137 (1986)].
[33] V. G. Solov'ev, Fiz. Elem. Chastits At. Yadra **9**, 860 (1978) [Sov. J. Part. Nucl. **9**, 343 (1978)].
[34] V. A. Khodel and E. E. Saperstein, Phys. Rep. **92**, 183 (1982).
[35] Dao Tien Khoa, Nucl. Phys. **A484**, 376 (1988).
[36] L. W. Put and A. M. J. Paans, Nucl. Phys. **A291**, 93 (1977).
[37] H. Dabrowski, A. Budzanowski, and O. Mayer-Boricke, Annual Report, Institut für Kernphysik der Kernforschungsanlage Jülich, 1979, p. 3.
[38] D. A. Goldberg, Phys. Lett. **55B**, 59 (1975).
[39] Dao Tien Khoa, O. M. Knyaz'kov, I. N. Kukhtina, and G. A. Feofilov, Yad. Fiz. **50**, 80 (1989) [Sov. J. Nucl. Phys. **50**, 50 (1989)].
[40] E. W. Schmid and K. Wildermuth, Nucl. Phys. **26**, 463 (1961).
[41] P. P. Zarubin, Izv. Akad. Nauk SSSR Ser. Fiz. **51**, 119 (1987) [Bull. Acad. Sci. USSR Phys. Ser. **51**, No. 1, 111 (1987)].
[42] J. P. Jeukenne, A. Lejeune, and C. Mahaux, Phys. Rep. **25**, 83 (1976).
[43] M. Kohno, D. W. Sprung, S. Nagata *et al.*, Phys. Lett. **137B**, 10 (1984).
[44] H. Eickoff, D. Frekers, H. Löhner *et al.*, Nucl. Phys. **A252**, 333 (1975).
[45] H. H. Chang, B. W. Ridley, T. H. Braid *et al.*, Nucl. Phys. **A270**, 413 (1976).
[46] K. B. Baktybaev, A. D. Duĭsebaev, and A. B. Kabulov, Izv. Akad. Nauk SSSR Ser. Fiz. **39**, 2151 (1975) [Bull. Acad. Sci. USSR Phys. Ser. **39**, No. 10, 123 (1975)].
[47] K. A. Gridnev and A. A. Ogloblin, Fiz. Elem. Chastits At. Yadra **6**, 393 (1975) [Sov. J. Part. Nucl. **6**, 158 (1975)].
[48] D. A. Goldberg, S. M. Smith, H. G. Pugh *et al.*, Phys. Rev. C **7**, 1938 (1973).
[49] R. Newton, *Scattering Theory of Waves and Particles*, 1st ed. (McGraw-Hill, New York, 1966) [Russ. transl., Mir, Moscow, 1969].
[50] H. M. Khalil, K. W. McVoy, and M. M. Shalaby, Nucl. Phys. **A455**, 100 (1986).
[51] K. W. McVoy, H. M. Khalil, and M. M. Shalaby *et al.*, Nucl. Phys. **A455**, 118 (1986).
[52] J. Knoll and R. Schaeffer, Ann. Phys. (N.Y.) **97**, 307 (1976).
[53] G. R. Satchler, Nucl. Phys. **A409**, 3 (1983).
[54] R. Pesl, H. J. Gils, H. Rebel *et al.*, Z. Phys. A **313**, 111 (1983).
[55] R. C. Fuller, Phys. Rev. C **12**, 1561 (1975).
[56] K. W. McVoy and G. R. Satchler, Nucl. Phys. **A417**, 157 (1984).
[57] R. C. Fuller and K. W. McVoy, Phys. Lett. **55B**, 121 (1975).
[58] Yu. A. Berezhnoĭ, A. V. Kuznichenko, G. M. Onishchenko *et al.*, Fiz. Elem. Chastits At. Yadra **18**, 289 (1987) [Sov. J. Part. Nucl. **18**, 121 (1987)].
[59] E. Stiliaris, H. G. Bohlen, P. Fröbrich *et al.*, Phys. Lett. **223B**, 291 (1989).
[60] A. S. Demyanova, J. M. Bang, F. A. Gareev *et al.*, Nucl. Phys. **A501**, 336 (1989).
[61] A. Nadasen, M. McMaster, M. Fingal *et al.*, Phys. Rev. C **39**, 536 (1989).
[62] A. S. Dem'yanova, Preprint IAÉ-4139/2, Kurchatov Institute of Atomic Energy (1985) [in Russian].
[63] Yu. A. Berezhnoĭ and V. V. Pilipenko, Dokl. Akad. Nauk SSSR **275**, 52 (1984) [Sov. Phys. Dokl. **29**, 202 (1984)].
[64] A. S. Demyanova, A. A. Ogloblin, Yu. V. Lyshko *et al.*, Phys. Rev. C **38**, 1975 (1988).
[65] S. N. Ershov, F. A. Gareev, R. S. Kurmanov *et al.*, Phys. Lett. **227B**, 315 (1989).
[66] J. Albinski, A. Budzanowski, H. Dabrowski *et al.*, Nucl. Phys. **A445**, 477 (1985).
[67] H. Rebel, R. Lohken, G. W. Schweimer *et al.*, Z. Phys. A **256**, 258 (1972).
[68] W. Karcz, L. Kluska, Z. Sarok *et al.*, Acta Phys. Pol. **B3**, 525 (1972).
[69] J. Alstel, Phys. Rev. **141**, 1138 (1966).
[70] H. J. Gils, H. Rebel, J. Buschmann *et al.*, Z. Phys. A **279**, 55 (1976).

[71] B. Tatischeff and I. Brissaud, Nucl. Phys. **A155**, 89 (1970).
[72] S. M. Smith, G. Tibell, A. A. Cowley *et al.*, Nucl. Phys. **A207**, 273 (1973).
[73] H. J. Gils, E. Friedman, H. Rebel *et al.*, Report KfK 2838, Kernforschungszentrum Karlsruhe, 1979.
[74] J. Cook, H. J. Gils, H. Rebel *et al.*, Nucl. Phys. **A388**, 173 (1982).
[75] G. R. Satchler, C. B. Fulmer, R. L. Auble *et al.*, Phys. Lett. **128B**, 147 (1983).
[76] J. S. Lilley, B. R. Fulton, M. A. Nagarajan *et al.*, Phys. Lett. **151B**, 181 (1985).
[77] S. C. Pieper, M. H. Macfarlane, D. H. Gloeckner *et al.*, Phys. Rev. C **18**, 180 (1978).
[78] J. B. Ball, C. B. Fulmer, E. E. Gross *et al.*, Nucl. Phys. **A252**, 208 (1975).
[79] C. Olmer, M. Mermaz, M. Buenerd *et al.*, Phys. Rev. C **18**, 205 (1978).
[80] R. O. Groeneveld, L. Meyer-Schultzmeister, A. Richter *et al.*, Phys. Rev. C **6**, 805 (1972).
[81] S. E. Vigdor, D. G. Kovar, P. Sperr *et al.*, Phys. Rev. C **20**, 2147 (1979).
[82] K. E. Rehm, W. Henning, J. R. Erskine *et al.*, Phys. Rev. Lett. **40**, 1479 (1978).
[83] H. Doubre, J. C. Jacmart, E. Plagnol *et al.*, Phys. Rev. C **15**, 693 (1977).
[84] R. C. Barrett and D. F. Jackson, *Nuclear Sizes and Structure* (Clarendon Press, Oxford, 1977) [Russ. transl., Naukova Dumka, Kiev, 1981].
[85] K. H. Bray, M. Jain, K. S. Jayaraman *et al.*, Nucl. Phys. **A189**, 35 (1972).
[86] G. R. Satchler, Phys. Lett. **83B**, 284 (1979); Nucl. Phys. **A329**, 233 (1979).
[87] Dao Tien Khoa, I. N. Kukhtina, and V. Yu. Ponomarev, Yad. Fiz. **44**, 906 (1986) [Sov. J. Nucl. Phys. **44**, 585 (1986)].
[88] M. A. Nagarajan, I. J. Thompson, and R. C. Johnson, Nucl. Phys. **A385**, 525 (1982).
[89] Y. Sakuragi, M. Yahiro, and M. Kamimura, Prog. Theor. Phys. **70**, 1047 (1983).
[90] C. B. Fulmer, G. R. Satchler, K. A. Erb *et al.*, Nucl. Phys. **A427**, 545 (1984).
[91] O. M. Knyaz'kov, I. N. Kukhtina, and G. A. Feofilov, Preprint R4-85-908, JINR, Dubna (1985) [in Russian].

Translated by Patricia Millard